Published in final edited form as:
*J Neurochem*. 2009 January ; 108(1): 231–245. doi:10.1111/j.1471-4159.2008.05758.x.

# Doublecortin induces mitotic microtubule catastrophe and inhibits glioma cell invasion

**Manoranjan Santra**[1], **Sutapa Santra**[1], **Cindi Roberts**[1], **Rui Lan Zhang**[1], and **Michael Chopp**[1,2]

[1] Department of Neurology, Henry Ford Health System, Detroit, MI 48202, USA

[2] Department of Physics, Oakland University, Rochester, MI 48309, USA

## Abstract

Doublecortin (DCX) is a microtubule binding protein that induces growth arrest at the G2-M phase of cell-cycle in glioma and suppresses tumor xenograft in immunocompromised hosts. DCX expression was found in neuronal cells, but lacking in glioma cells. We tested the hypothesis that DCX inhibits glioma U87 cell mitosis and invasion. Our data showed that DCX synthesizing U87 cells underwent mitotic microtubule spindle catastrophe in a neurabin II dependent pathway. Synthesis of both DCX and neurabin II were required to induce apoptosis in U87 and HEK 293T cells. In DCX expressing U87 cells, association of phosphorylated DCX (P-DCX) with protein phosphatase-1 (PP1) in the cytosol disrupted the interaction between kinesin-13 and PP1 in the nucleus and yielded spontaneously active kinesin-13. The activated kinesin-13 caused mitotic microtubule catastrophe in spindle checkpoint. P-DCX induced depolymerization of actin filaments in U87 cells, downregulated matrix metalloproteinase -2 (MMP-2) and MMP-9, and inhibited glioma U87 cell invasion in a neurabin II dependent pathway. Thus, localization of the DCX-neurabin II-PP1 complex in the cytosol of U87 tumor cells inhibited PP1 phosphatase activities leading to anti-glioma effects via 1) mitotic microtubule spindle catastrophe that blocks mitosis, and 2) depolymerization of actin that inhibits glioma cell invasion.

### Keywords

Doublecortin; glioma; mitotic catastrophe; mitosis; actin; invasion

## Introduction

Gliomas, the most malignant intracranial tumors rapidly invade the brain. All treatments for glioma such as surgery, radiotherapy, and chemotherapy fail (Reviewed in ref. Demuth *and* Berens 2004). We therefore seek agents that suppress glioma tumor growth as well as inhibit glioma cell invasion into the brain. Doublecortin (DCX), a gene that is absent from glioma cells, suppresses glioma (Santra *et al.*, 2006a). DCX interacts with spinophilin/neurabin II, a tumor suppressor, and PP1, one of the key eukaryotic serine/threonine protein phosphatases. These interactions lead to inhibition of proliferation and anchorage independent growth of glioma cells (Santra *et al.*, 2006a). Inactivation of PP1 by okadaic acid blocks mitosis (Yamashita *et al.*, 1990). The microtubule (MT) associated proteins (MAPs) such as DCX, *Von Hippel Lindau* (pVHL) and MAP2 are either absent or mutated in many tumor cells including glioma and function as tumor suppressor genes (Soltani *et al.*, 2005, Santra *et al.*,

Address Correspondence to Michael Chopp, Neurology Research, Henry Ford Hospital, Education and Research Building, Room 3056, 2799 West Grand Boulevard, Detroit, MI 48202. chopp@neuro.hfh.edu, Telephone: 313-916-3936, Fax: 313-916-1318.

2006a). The dynamic instability of MTs in mitotic spindle checkpoint is a critical step during mitosis and is regulated by kinases and phosphatases (reviewed in ref. Gadde and Heald 2004). To our knowledge, there is no report regarding the effect of DCX on the dynamic instability of MTs in mitotic spindle checkpoint in glioma cells and on glioma invasion.

DCX is expressed in clusters of neuroblasts in the area between the subventricular zone (SVZ) and the tumor and expression is highest in proximity to the SVZ (Bexell *et al.*, 2007). DCX synthesis induces expression of neuronal markers such as nestin and MAP-2 at the protein and mRNA levels in glioma U87 cells, as previously reported (Santra *et al.*, 2006b). In our present study, we found that DCX is absent in human and rodent glioma, but is expressed in the peritumor region of human and rodent glioma. DCX blocked mitosis by inducing catastrophe of MTs in mitotic spindle checkpoint and inhibited glioma cell invasion by inducing actin depolymerization via a novel neurabin II/PP1 dependent pathway.

## Materials and Methods

### Cell cultures

Human glioblastoma U87, human embryonic kidney 293T (HEK 293T), rat astrocytes, PC-12, mouse Cath.a neurons and mouse cerebral endothelial were obtained from American Type Culture Collection (ATCC), Manassas, VA. Human primary glioblastoma multiforme (PGM-YU) were generously provided by Dr. Anthony N. van den Pol, Department of Neurosurgery, Yale University School of Medicine, New Haven, Connecticut (Ozduman *et al.*, 2008). Human low grade astrocytoma (HF29), human primary glioblastoma multiforme (HF66) and human anaplastic astrocytoma (HF69) cells were obtained from Dr. Thomas Mikkelsen, Henry Ford Hospital, Detroit, MI. Mouse oligodendrocytes were provided by Dr. Anthony Campagnoni, University of California, Los Angeles, CA (Zhang *et al.*, 2008). Rat subventicular zone (SVZ) cells were prepared and maintained including all cells, as previously described (Santra *et al.*, 2006b, 2006c). The DCX expressing U87 and 293T clones were generated, as previously reported (Santra *et al.*, 2006a). Commercially available plasmids containing either neurabin II siRNA or MMP2siRNA or MMP9siRNA cassettes (Santa Cruz Biotechnology, Santa Cruz, CA) were transiently transfected in control and DCX synthesizing U87 and HEK293T cells, as previously described (Santra *et al.*, 2006a). Preparation of DCXsiRNA with targeted sequences in lentiviral vectors containing green fluorescent protein (GFP) expression cassette and treatment of DCXsiRNAs in control and DCX synthesizing U87 and HEK293T cells were previously described (Santra *et al.*, 2006b).

### U87 cell implantation

U87 and *Discosoma* red fluorescent protein-2 (DsRed-2) expression vector pIRES2-DsRed-2 (Clontech Laboratories, Inc. Mountain View, CA) stably transfected U87 cells were implanted into the striatum of male nude rats (250–300 g) ($5\times10^5$cells/rat) at the following location: bregma +1 mm; lateral +3 mm; ventral −4 mm on day 1, as previously described (Santra *et al.*, 2006a; Zhang *et al.* 2006). The rats were sacrificed on day 14 after tumor implantation. Each forebrain from animals was cut into 7 coronal blocks. Brains were snap frozen and sectioned at a thickness of 8 microns into ~10 slides for each adjacent coronal block as previously described (Ahn *et al.*, 1999).

### Preparation of paraffin-embedded section

Nude rats were anesthetized, the vascular system transcardially perfused with heparinized saline followed by 4% paraformaldehyde and sacrificed. Each forebrain from animals was cut into 7 coronal blocks and then embedded with paraffin. A series of adjacent 6 μm-thick sections (~20) were cut from each block and one section from each block stained with hematoxylin and eosin (H&E), as previously described (Santra *et al.*, 2006a; Zhang *et al.*, 2004).

## Immunohistochemistry

The immunohistochemistry of paraffin-embedded sections was performed by conventional deparaffinization and dehydration sequence, as previously described (Santra *et al.*, 2006a; Zhang *et al.,* 2004). The cells were seeded in 8-well chamber slides (Lab-Tek, Nunc, Inc., Naperville, IL) and immunostained, as previously described (Santra *et al.*, 2008, 1997). The slides from frozen sections, deparaffinized paraffin sections and cells in culture were blocked with normal serum, incubated with primary antibodies for 1 hr, washed for several times and incubated with secondary antibodies labeled with either 3,3′-Diaminobenzidine (DAB) (brown staining), fluorescein isothiocyanate (FITC) (green fluorescence) or cyanine fluorophore (Cy3) (red fluorescence) for 1 hr. The slides were counterstained with 4′, 6-diamidino-2-phenylindole (DAPI) (blue fluorescence) and examined under Fluorescent Illumination Microscope (Olympus IX71/IX51, Tokyo, Japan).

Goat antiserum for DCX (1:500; Santa Cruz Biotechnology, Santa Cruz, CA), polyclonal rabbit anti-class III β-tubulin (TUJ1) and mouse polysialic acid on neural cell adhesion molecule (PSA-NCAM) (1:500, Chemicon, Temecula, CA), monoclonal antibodies for MAP2 (1:1000), α-tubulin (1:500; Sigma, Saint Louis, Missouri), kinesin-13 and PP1 (1:1,000; Santa Cruz Biotechnology, Santa Cruz, CA) were used as primary antibodies, and labeled with either anti-goat or anti-mouse secondary antibodies (1:5,000) conjugated with either FITC or Cy3 (1:5,000; Santa Cruz). The slides were counterstained with or without DAPI and examined by using a Fluorescent Illumination Microscope (Olympus IX71/IX51, Tokyo, Japan). The actin stress fibers were stained with fluorescein isothiocyanate-phalloidin (Fl-phalloidin) according to the manufacturer's protocol (Sigma). Each experiment was repeated at least three times.

## Quantitative real time PCR

Absolute quantitative real time PCR (qrtPCR) was performed to measure mRNA transcripts according to method of Garzon et al. (Garzon and Fahnestock 2007). Standard curves for DCX, neurabin II, green fluorescence protein (GFP) and glyceraldehyde-3-phosphate dehydrogenase (GAPDH) transcripts were made from their cDNA inserted into plasmids (Santra *et al.* 2006a–c, Santra *et al.* 1997) with ten 10-fold serial dilutions starting at $1.0\times10^{3}$ copies of cDNAs. In the standard curve, the primers without templates and templates without primers were used as negative controls. The copies of cDNAs were calculated based on Avogadro's number according to Monnet et al. (Monnet et al. 2006). The $1.0\times10^{-3}$ copies was the detection limit for each primer set used in qrtPCR for all plasmid templates and the copies of transcripts evaluated by linear standard curve. The transcripts are not detectable for the templates containing less than $1.0\times10^{-3}$ copies. Total RNA extraction and cDNA synthesis were performed and all DNA primers used, as previously described (Santra *et al.,* 2006a–c). Total RNA from HEK 293T cells was used as a negative control for DCX expression (Shmueli *et al.,* 2006). For PCR amplification, the 40 cycles had the following thermal profile: 95°C for 30 s, 58°C for 30 s, and 72°C for 45 s. After PCR, dissociation curves and agarose gel electrophoresis were performed to verify the quality of the PCR products. There were no secondary products. Results were expressed as copies per nanogram (ng) of total RNA. Expression of matrix metalloproteinase 2 (MMP2), MMP9, MMP14 and β-actin were analyzed by relative qrtPCR based on the comparative threshold cycle (ct) method also referred to as the $2^{-\Delta\Delta CT}$ method in five independent experiments (Livak and Schmittgen 2001).

## Fluorescence-activated cell sorting (FACS) analysis

In order to estimate what percentage of total brain cells expressed DCX, FACS analysis of DCX expressing cells in total brain cells from nude rat (n=4) was performed according to method of Liu et al. with slight modification (Liu et al. 2006). The brain cells were prepared by using the protocol for subventical zone cell preparation, as previously described (Santra et al. 2006b, 2006c). The brain cells were immunostained with goat antiserum for DCX (1:1,000;

Santa Cruz Biotechnology) for 2h, washed the cells with PBS for 5 times and labeled with anti-goat secondaryantibody (1:5,000) conjugated with FITC for 1h. The cells were washed the cells with PBS for 5 times. In order to investigate the cell cycle, fluorescence-activated cell sorting (FACS) analysis was performed by dual labeling the cells with bromodeoxyuridine (BrdUrd) and propidium iodide in BD FACSCalibur Flow Cytometer (BD Bioscience, Qume Drive, San Jose, CA), as previously described (Santra et al. 2006a).

### TUNEL assay and Cell proliferation assay

TUNEL stains were performed by using the Apoptosis Detection Kit, ApopTag Fluorescein according to the manufacturer's protocol (Intergen Company, Purchase, NY, USA), as previously described (Santra *et al.*, 2006b, c). The CellTiter 96 Aqueous Non-Radioactive Cell Proliferation Assay (Promega Corporation, Madison, WI, USA) was used to determine the number of viable cells in the proliferative phase, according to the manufacturer's protocol (Santra *et al.*, 1995).

### Immunochemical procedures

Total brain tissue extracts from the normal nude rat brain were prepared according to method of Romanic *et al.* (Romanic *et al.*, 1998). The protein extracts were separated by SDS-PAGE for Western blot analysis. Immunoprecipitation, Western blot analysis, calf intestinal alkaline phosphatase (Promega, Madison, Wisconsin, USA) treatment at dose of 1U/μg of protein for 30 min, treatment with c-jun NH2-terminal kinase (JNK) specific inhibitor II (SP600125) (Calbiochem, San Diego, CA, USA) at the dose of 1 μM for 3h were performed, as previously described (Santra *et al.*, 2006a; 2000; 1997; 1995). For Western blot analysis, goat antiserum for DCX (1:1,000), monoclonal antibodies (1:1,000) for kinesin-13 and PP1, rabbit anti-neurabin-II polyclonal antibody (1:1,000; Upstate, Charlottesville, VA), mouse monoclonal MMP2, MMP9, β-actin (1:1,000–5,000; Santa Cruz Biotechnology), MMP14 (1:1000; Chemicon, Temecula, CA) and rabbit anti-JNK1 polyclonal antibody (1:2,000; Promega, Madison, WI) were used. Donkey anti-goat, antirabbit and antimouse horseradish peroxidase (1:10,000; Jackson ImmunoResearch Labs, West Grove, PA) were used as secondary antibodies. Each experiment was repeated at least three times. Zymography of MMP2 and MMP9 was performed, as previously described (Santra *et al.*, 2008).

### Matrigel invasion assay

Matrigel invasion assay was performed in the presence of serum according to the method of Jiang *et al.* (Jiang *et al.*, 2002). Briefly, $10^5$ cells were seeded on the upper well of Biocoat Matrigel chambers (8 μm pore size; Becton Dickinson). After 24 h for U87 cells and 72 h for HEK 293T cells, the invading cells on the underside of the filters were stained with DAPI, and four fields were counted for each of the replicate membranes. Each experiment was repeated at least three times.

### Quantitative scrape migration assay

Quantitative scrape migration assay was performed, as previously described (Santra *et al.*, 2006b), with slight modification. The 6 scrapes were made at random by scratching with a sterile 1000 μl microliter pipette tip. Photographs of 6 scrapes were taken at 0, 6 and 12 hours after scraping. Each experiment was repeated at least three times.

### Statistical analysis

One-way ANOVA followed by Student-Newman-Keuls test was used. The values were the mean of 5 to 10 independent experiments for real-time PCR data and three independent experiments for Western blot analysis. The data are presented as mean ± SD. $P < 0.05$ is considered as significant.

## Results

### DCX expression is lacking in glioma tumor

DCX expression was not detected in different glioma cell lines, as previously reported (Santra *et al.*, 2006a). However, DCX mRNA was determined by relative qrtPCR in different glioma cell lines. In relative qrtPCR, $2^{-\Delta\Delta CT}$ value was arbitrarily accepted as 1 for glioma cells indicating reproducibly detected delta CT value. However, undetected PCR products in Agarose gel and undetected DCX protein in Western blot analysis indicate that DCX expression is absent in glioma cell lines (Santra *et al.*, 2006a). The actual ct values for glioma cells were of undermined range (>38). In order to avoid confusion in DCX mRNA expression in glioma cells, absolute qrtPCR was performed instead of relative qrtPCR. To investigate DCX expression, normal human brain RNA samples (20–50 years old donors; Cat. 540135, 540143, 540137; Stratagene, La Jolla, CA) and primary human brain tumor RNA samples from PGM-YU, HF66, HF69 and HF29 cells grown in culture up to 30 passages in order to minimize or eliminate normal cells were analyzed by absolute qrtPCR (Fig. 1a). DCX mRNA transcripts were not detected in primary glioma PGM-YU, HF66, HF69 and HF29 cells. In contrast, DCX mRNA transcripts were detected in normal human brain RNA samples (Fig. 1a). GAPDH mRNA transcripts were consistently detected both in normal human brain and primary glioma cells. For Western blot analysis, normal human brain protein extract (Cat. 635301, Clontech Laboratories, Inc. Mountain View, CA) was intentionally loaded 10 times lower protein concentration (20μg) than each primary human brain tumor cells (200 μg) in order to avoid antibody sensitivity and exposure discrimination and exposed for overnight (Fig. 1b). None of the primary glioma cells showed any protein band (Fig. 1b). DCX protein bands were quantified by histogram analysis of Western blot in Photoshop for 100μg proteins from control and the primary glioma cells in three independent experiments (Santra *et al.* 2006c). These primary human brain tumors PGM-YU, HF66, HF69 and HF29 cells did not express DCX at the mRNA and protein levels (Fig. 1a, b and c). In contrast, DCX was detected in normal human brain. In order to estimate what percentage of total brain cells express DCX, FACS analysis was performed in total brain cells from nude rat according to method of Liu *et al.* (Liu *et al.* 2006). We found that 1.17± 0.11% cells were DCX positive in total brain cells. To identify where DCX is expressed in brain, paraffin sections of normal nude rat brain were immunostained with DCX antibody labeled with DAB. The sub-ventricular zone (SVZ) lining the lateral ventricle (LV) was the only region stained for DCX (Fig. 2a). To confirm DCX expression in the SVZ, SVZ cells were isolated, extracted for proteins and analyzed by Western blot including whole brain, astrocytes, mouse oligodendrocytes, PC-12, CATH.a neurons and mouse cerebral endothelial cell protein extracts, as previously described (Santra *et al.*, 2006b; 2006c). DCX expression was detected only in whole brain and SVZ cell protein extracts (Fig. 2b). SVZ cells expressed DCX at a higher level than whole brain (Fig. 2b). To detect cell types, double immunofluorescence stainings were performed in the SVZ region of paraffin sections of nude rat brain with the neuronal markers MAP2, TUJ1 and PSA-NCAM (Santra *et al.* 2006b; Corbo *et al.* 2002; Bexell *et al.* 2007). The alternate slides corresponding to immunostaining regions were also stained with H&E (Fig. 2c). Double immunofluorescence stainings revealed that DCX was co-expressed with all three neuronal markers MAP2, TUJ1 and PSA-NCAM (Fig. 2c). These data indicate that DCX was highly expressed in neuronal SVZ cells. To examine DCX expression in human glioma tissue, we immunostained the paraffin embedded sections of human glioblastoma multiforme (14 slides), astrocytomas (8 slides) and oligodendrogliomas (15 slides) (obtained from Dr. T. Mikkelsen, Henry Ford Hospital, Detroit, MI) with DCX antibodies. DCX was only detected in peri-tumor region of human glioblastoma multiforme (4 slides), astrocytomas (2 slides) and oligodendrogliomas (8 slides) in 14 out of 37 slides and also in peritumor region of implanted U87 tumor in nude rats (Fig. 3). Double immunofluorescence stainings demonstrated cellular co-localization of the neuronal markers MAP2, TUJ1 and PSA-NCAM with DCX in peritumor region of glioma

(Fig. 3). To analyze whether glioma tumor cells express DCX in vivo, U87 cells were labeled with DsRed-2 and implanted in nude rats. The rats were sacrificed on day 14 after tumor implantation. The frozen sections were analyzed by immuno fluorescence staining for DCX expression. There were no DCX positive cells detected within the tumor. In contrast, there were some DCX expressing cells residing just outside of the tumor (Fig. 4). These data indicate that glioma tumor cells did not express DCX.

### DCX synthesis induces microtubule catastrophe in mitotic spindle checkpoint in vitro

DCX is a MT binding protein (Taylor *et al.*, 2000). MTs are essential for a wide variety of cellular functions including mitosis and cell motility (Reviewed in ref. Jackson *et al.*, 2007, Bruce Bowerman 2004). DCX synthesis causes growth arrest in the G2-M phase of cell cycle progression (Santra *et al.*, 2006a). Ionizing radiation, pharmaceutical agents- okadaic acid, geldanamycin, temozolomide and tumor suppressor gene - p53 induce growth arrest in G2-M phase of cell cycle and mitotic catastrophe in cancer cells including glioma by interfering MTs (Eriksson *et al.*, 2007; Yamashita *et al.*, 1990; Nomura *et al.*, 2004; Hirose *et al.*, 2005; Ianzini *et al.*, 2007). We therefore studied the effect of DCX on mitotic catastrophe in glioma U87 and HEK 293T cells, as described (Nomura *et al.*, 2004). To examine mitotic catastrophe, the cells were grown to mitotic stage on glass coverslips for 30 hours, fixed and immunostained for the mitotic tubulins of mock and DCX transfected glioma U87 cells to visualize the pattern of microtubules, spindles and centrosomes, as previously described (Santra *et al.*, 2006b). These data were quantified by counting the dividing cells with classic bipolar spindle poles for mitosis as well as multinuclear giant cells in 3 independent experiments. We found that the mock-transfected glioma U87 and HEK293T cells, and DCX transfected neurabin II null HEK293T cells showed that nearly all cells contained a nucleus with mitotic MTs and classic bipolar spindle poles (Fig. 5a,b, 7). In contrast, the majority of DCX transfected U87 cells were large multinucleated cells with multipolar spindle poles (Fig. 5a, 7). Synthesis and knock down of DCX and neurabin II, and GFP expression were confirmed by absolute qrtPCR and Western blot in U87 and HEK 293T cells (Fig. 6a, b). The formation of multinuclear giant cells or cells with several micronuclei is referred to as a “mitotic catastrophe” (Eriksson *et al.*, 2007; Yamashita *et al.*, 1990; Nomura *et al.*, 2004; Hirose *et al.*, 2005; Ianzini *et al.*, 2007). These data suggested that DCX and neurabin II expressing cells underwent mitotic catastrophe. To confirm the involvement of neurabin II on mitotic catastrophe, re-expression of neurabin II in HEK 293T cells by transiently transfecting with neurabin II expression vector (Santra *et al.*, 2006a) and knock down of neurabin II by siRNA transfection in U87 cells were performed. DCX or neurabin II synthesis alone had no effect on mitotic MTs catastrophe in U87 and HEK 293T cells (Fig. 5a,b, 7). In contrast, synthesis of both DCX and neurabin II induced mitotic MTs catastrophe in U87 and HEK 293T cells (Fig. 5a,b, 7). These data demonstrated that both DCX and neurabin II were required to induce mitotic MTs catastrophe in the mitotic spindle checkpoint and to block the mitosis of the U87 and HEK 293T cells.

### DCX and neurabin II synthesis induce apoptosis in U87 and HEK 293T cells

Mitotic catastrophe is the modality of apoptosis leading to the formation of large non-viable cells with several micronuclei containing uncondensed chromosomes (Reviewed in ref. Castedo *et al.*, 2002). We therefore investigate the effect of DCX and neurabin II synthesis on apoptosis by TUNEL staining, cell cycle by FACS analysis and proliferation assay in U87 and HEK 293T cells. DCX transfection had no significant effect on TUNEL staining in U87 and HEK 293T cells (Fig. 8a). Double transfection with DCX and neurabin II induced apoptosis in U87 and HEK 293T cells (Fig. 8a). Either DCX or neurabin II transfection significantly induced growth arrest in G2-M phase of cell cycle progression and also significantly suppressed proliferation in U87 cells (Fig. 8b, c). Combined transfection of DCX and neurabin II influenced the effect on growth arrest in G2-M phase of cell cycle and growth suppression in U87 cells (Fig. 8b, c). In contrast, DCX and neurabin II combined transfection was required

for significant effect on growth arrest in G2-M phase of cell cycle and on growth suppression in HEK 293T cells (Fig. 8b, c). These data indicate that synthesis of both DCX and neurabin II induced apoptosis in U87 and HEK 293T cells.

## DCX synthesis inhibits association and activity of protein phosphatase type-1 (PP1) for kinesin-13

Activation of depolymerizers causes catastrophe of mitotic spindle and blocks the G2-M phase in the cell cycle progression (Gadde and Heald 2004). DCX bound MTs are substrates for depolymerising kinesins such as kinesin-13 (Moores *et al.*, 2006a). To determine the mechanism of DCX induced MT catastrophe, we performed a sequential immuno precipitation (IP) and Western blot analysis from total cell lysates of the same cells that were used for catastrophe analysis (Fig. 5, 6). Interaction of DCX with kinesin-13 (a major MT depolymerizer) (Moores *et al.*, 2006b), PP1 (a key inactivator of MT depolymerizer) (Alphey et al. 1997, Bruce Bowerman 2004) and neurabin II was analyzed. To analyze the effect of phosphorylation in DCX on protein-protein interaction, the cells were treated with a JNK specific inhibitor, as previously described (Santra *et al.*, 2006a). The cell lysates were treated with an alkaline phosphatase to dephosphorylate DCX, as previously described (Santra *et al.*, 2006a). Sequential IP and Western blot analysis for PP1 and kinesin-13 revealed that kinesin-13 did not interact with PP1 in DCX transfected U87 cells (Fig. 9a). In contrast, kinesin-13 interacted with PP1 either in DCX negative or neurabin II negative or DCX positive but neurabin II negative U87 and HEK 293T cells (Fig. 9a). The dephosphorylated DCX samples showed interaction of kinesin-13 and PP1 in U87 and HEK 293T cells (Fig. 9a). Phosphorylated DCX (P-DCX) was also associated with neurabin II and PP1 in DCX synthesizing U87 cells (Fig. 9a). P-DCX therefore acted as a competitive inhibitor of PP1 for interaction between kinesin-13 and PP1. To study involvement of DCX phosphorylation in protein-protein interaction, U87 and HEK 293T cells were transiently transfected with expression vectors containing dominant negative acting mutants of JNK1 (generously provided by Dr. Roger Davis, Biochemistry and Molecular Pharmacology, University of Massachussets Medical School, Worcester, Massachusetts; ref. Raingeaud *et al.*, 1995) as well as constitutively active expression vector of JNK 1 fused with MKK7 (Santra *et al.*, 2006a). To confirm whether neurabin II was required for protein/protein interaction, neurabin II was overexpressed in U87 cells and re-expressed in HEK 293T cells by transfection with neurabin II expression vector. Expression of dominant negative JNK1 mutant, active JNK 1 fused with MKK7, neurabin II and DCX were analyzed by Western blot in U87 and HEK 293T cells (Fig. 9b). The dephosphorylation of DCX by dominant negative JNK1 mutant transfection induced interaction of kinesin-13 and PP1 in DCX and neurabin positive U87 and HEK 293T cells (Fig. 9b). The phosphorylation of DCX by active JNK 1-MKK7 transfection induced association of PP1 with neurabin II and DCX and abolished interaction of PP1 with kinesin-13 in DCX and neurabin II synthesizing U87 and HEK 293T cells (Fig. 9b). In DCX and neurabin II synthesizing U87 and HEK 293T cells, kinesin-13 remained phosphorylated as an active form and caused catastrophe in the mitotic spindle checkpoint leading to growth arrest in the G2-M phase of the cell cycle progression in a novel neurabin II dependent pathway.

## PP1 localizes in the cytosol of DCX transfected U87 cells

Physical interaction between kinesin-13 and PP1 is necessary to inactivate kinesin-13 (Alphey et al. 1997, Bruce Bowerman 2004). The cellular localization of PP1, therefore, plays an important role in regulation of kinesin-13. In DCX synthesizing cells, PP1 is associated with neurabin II and DCX, and colocalized in the cytosol (Shmueli *et al.*, 2006). To confirm the cellular localization of PP1 and kinesin-13, the mock and DCX transfected U87 and HEK293T cells were immunostained for PP1, kinesin-13 and DCX. We found that PP1 colocalized with kinesin-13 in the nucleus of control U87 cells (Fig. 10a). In contrast, PP1 mostly localized in the cytosol and kinesin-13 localized in the nucleus of DCX transfected U87 cells (Fig. 10a).

PP1 and kinesin-13 were colocalized in the nucleus of control and DCX transfected HEK 293T (neurabin II null) cells (Fig. 10a). PP1 colocalized with DCX in the cytosol of DCX transfected U87 cells (Fig. 10b). PP1 is therefore not available to interact and dephosphorylate (inactivate) kinesin-13 localized in the nucleus. Thus, kinesin-13 remains active and induces catastrophe in mitotic spindles that leads to growth arrest in G2-M phase of cell cycle.

### DCX synthesis induces actin depolymerization in DCX transfected U87 Cells

As PP1 also plays a major role in actin polymerization (Gu *et al.*, 2003; Oliver *et al.*, 2002) and colocalizes with two actin binding proteins DCX and neurabin II (Bielas *et al.*, 2007; Tsukada *et al.*, 2006) in the cytosol, we therefore investigated the effect of DCX on actin dynamics by utilizing the mock and DCX transfected U87 and HEK293T cells (shown in Fig. 6a,b) for actin staining. Actin filaments disappeared and underwent degradation in DCX synthesizing U87 cells (Fig. 11a). In contrast, control U87 cells and HEK293T cells transfected with or without DCX contained actin filaments (Fig. 11a). DCXsiRNA transfection reversed the DCX effect on actin degradation in U87 cells (Fig. 11a). To confirm the involvement of neurabin II in actin degradation, knockdown of neurabin II by neurabin II siRNA transfection in DCX synthesizing U87 cells and re-expression of neurabin II in DCX synthesizing HEK 293T cells shown in Fig. 6a,b were utilized for actin staining. The neurabin II siRNA transfection in DCX synthesizing U87 cells reversed DCX mediated actin degradation and re-established actin filament (Fig. 11a). The re-expression of neurabin II in DCX synthesizing HEK 293T cells induced actin filament degradation (Fig. 11a). To determine whether DCX phosphorylation plays a role in actin filament degradation, DCX expressing U87, and DCX and neurabin II overexpressing HEK 293T cells were transfected either with constitutively active JNK1-MKK7 expression vector or dominant negative acting JNK1 mutant expression vector (Fig. 9b). We found that JNK1-MKK7 transfection increased the degradation of actin filaments in DCX and neurabin II synthesizing U87 and HEK 293T cells (Fig. 11a). In contrast, the dominant negative acting JNK1 mutant transfection inhibited the degradation of actin filaments and re-formed actin filaments in DCX and neurabin II positive U87 and HEK 293T cells (Fig. 11a). These data indicated that phosphorylated DCX induces actin depolymerization in the presence of neurabin II in U87 cells.

### DCX synthesis suppresses expression and activation of MMP2 and MMP9

Dynamic alterations in the organization of the actin cytoskeleton play a critical role in tumor-associated progression such as invasion and metastasis (Chintala *et al.*, 1999; 1997). Inhibition of phosphatase activities induces actin depolymerization, reduces invasion of glioma cells and decreases matrix metalloproteinase (MMP) expression (Chintala *et al.*, 1999; 1997). MMPs promote tumor cell invasion (Blázquez *et al.*, 2008). To determine the involvement of DCX in glioma cell invasion, we analyzed the effect of DCX on expression and activation of known glioma invasion associated MMPs such as MMP2, MMP9 and MMP14 in glioma U87 and HEK 293T cells including a known player CD44 involved in glioma invasion (Blázquez *et al.*, 2008; Reviewed in ref. Bellail *et al.*, 2004). We found that DCX transfection reduced expression of MMP2 and MMP9 at the mRNA and protein levels (Figure 11b). In contrast, DCX had no effect on expression of MMP14 and CD44 at mRNA level (Fig. 11b). DCX synthesis also inhibited the activation of MMP2 and MMP9 based on zymography analysis (Figure 11c). In contrast, DCX transfection had no effect on activation of MMP14 in U87 cells (Fig. 11c).

### DCX synthesis inhibits U87 cell invasion in neurabin II dependent and independent pathways

To study the role of DCX on glioma cell invasion, U87 and HEK293T cells subjected to sequential DCX, neurabin II and their siRNAs transfections (Fig. 6a,b) were utilized for matrigel invasion assay. As U87 and HEK 293T cells showed different rate of invasion, we

therefore performed invasion assay in U87 cells for 24h and HEK 293T cells for 72h. DCX synthesis significantly reduced cell invasion in HEK 293T and U87 cells (Fig. 12). To investigate the involvement of MMP2 and MMP9 in DCX mediated inhibition of U87 cell invasion, MMP2siRNA and MMP9siRNA transfected U87 cells (Fig. 11c) were utilized for matrigel invasion assay. Single and combined MMP2siRNA and MMPsiRNA treatments were less efficient than DCX mediated inhibition of U87 cell invasion (Fig. 12). The absence of neurabin II did not reverse DCX inhibitory effect on cell invasion (Fig. 12). To study the importance of phosphorylation of DCX in glioma invasion, DCX synthesizing cells treated with JNK1 inhibitor, transfected with dominant negative mutant of JNK1 and constitutively active JNK1-MKK7 (Western blot analysis shown in Fig 9a,b) were used for matrigel invasion assay. We found that inhibition of phosphorylation on DCX reversed the inhibitory effect of DCX on U87 cell invasion (Fig. 12). In contrast, activation of phosphorylation on DCX induced the inhibitory effect of DCX on U87 cell invasion (Fig. 12). These data demonstrate that phosphorylation on DCX was required for DCX mediated U87 cell invasion. The scrape migration assay and its quantitative analysis based histogram (Santra *et al.,* 2006b) indicated that migration of DCX synthesizing U87 cells stopped after 6h, while control U87 cells continued migrating and filled the scrape by 12h (Fig. 13, 14). DCX siRNA transfection in DCX synthesizing U87 cells reversed the inhibitory effect of DCX on U87 cell migration (Fig. 13, 14). These data indicated that DCX suppresses U87 cell invasion.

## Discussion

Our present data showed that both human primary glioma cell culture and human glioma tissue were DCX deficient. DCX suppressed U87 glioma tumor in nude rats, as previously reported (Santra *et al*., 2006a). Here, we demonstrated that DCX significantly inhibited U87 cell invasion in vitro. We identified a novel mechanistic link to DCX mediated U87 tumor suppression and inhibition of U87 cell invasion via phosphorylation of DCX and DCX-PP1 interaction in the cytosol. Phosphorylated DCX blocked mitosis in U87 cells by inducing catastrophe of mitotic spindles via DCX-PP1 interaction in the cytosol. The phosphorylation of DCX and DCX-PP1 interaction also enhanced actin depolymerization that led to inhibition of U87 cell invasion.

We found DCX expression in peritumor regions of human and rat U87 glioma tumor. DCX is a member of an expanding family of MAPs, a class of MT polymerizers such as MAP2/tau and XMAP215. However, DCX has no sequence or structural homology with other MAPs. In contrast, DCX bound MTs are substrates for kinesin-13, a major MT depolymerizer (Moores *et al.,* 2006a). Kinesin is activated by kinesin-associated phosphoprotein (KAPP) upon phosphorylation in vivo and in vitro, and inactivated by a major dephosphorylating enzyme, protein phosphatase type 1 (PP1) upon dephosphorylation (Moores *et al.,* 2006b; Alphey et al. 1997, Bruce Bowerman 2004). To complete mitosis in the cell cycle, the level of expression, activation and inactivation of MT polymerizers and depolymerizers are required to be balanced (Gadde and Heald 2004). Therefore, a series of phosphorylation and dephosphorylation reactions are intimately involved with the regulation of mitotic processes such as spindles breakdown and re-formation (Gadde and Heald 2004). Here, we demonstrated that phosphorylated DCX being a substrate of PP1 interacts with PP1, colocalizes in the cytosol and prevents association between kinesin-13 and PP1 in the nucleus. As a result, kinesin-13 remains active and induces MT catastrophe in the mitotic spindle check point in a novel neurabin II dependent pathway. DCX synthesis induced mitotic spindle catastrophe. However, the multi-nucleated giant cells indicate that such cells with mitotic catastrophe may result from failure of cytokinesis without spindle defects (Huang et al. 2008). Alternatively, cell fusion may produce the multinucleated cells upon DCX synthesis (Reviewed in ref. Vile RG 2006). These data also warrant further investigation on effect of DCX synthesis on the failure of cytokinesis and induction of cell fusion. MT is one of the major targets of drug development.

Consequently, MT inhibitors have attracted great attention as anticancer agents for chemotherapeutic use (Reviewed in ref. Jackson *et al.*, 2007). DCX as an agent that targets MTs, may be a potential treatment for glioma. The distinct mechanism in which DCX interferes with mitosis provides the potential to overcome certain limitations of current tubulin-targeted anti-mitotic drugs and also to expand the scope of clinical efficacy that those drugs have established. DCX also serves as a unique tool to dissect the molecular mechanisms of the mitotic-checkpoint response. This finding of DCX action on mitosis could be the advent of molecularly targeted drug discovery for a new generation of anti-mitotic therapies that target proteins with specific functions in mitosis.

DCX is expressed in migrating neuroblasts (Francis *et al.*, 1999; Gleeson *et al.*, 1999). However, the function of DCX in migrating neuroblasts is not known. Mutations in the human doublecortin gene (DCX) cause profound defects in cortical neuronal migration, although genetic deletion of DCX in mice produces a milder defect (Corbo *et al.*, 2002). SVZ cells express DCX and migrate toward tumor, as previously reported (Santra *et al.*, 2006a, 2006b, Glass *et al*,. 2005, Zhang *et al.*, 2004). Interestingly, we were unable to detect DCX expression in any brain cell lines except SVZ cells. These data are also consistent with recently published data indicating that DCX is not detected in nonneoplastic glial cells in the adult brain, including astrocytes, oligodendrocytes, and microglia (Masui *et al.*, 2008). Masui *et al.* and Daou *et al.* suspected that glioma cells express DCX (Masui *et al.*, 2008; Daou *et al.*, 2005). However, they did not use any marker for neuron or glioma to confirm these DCX positive cells (Masui *et al.*, 2008, Daou *et al.*, 2005). To address this discrepancy of DCX expression in glioma, we immunostained paraffin sections of glioma tumor tissues with three neuronal markers MAP2, TUJ1 and PSA-NCAM along with DCX. Our data strongly indicate that DCX positive cells in peritumor region were neuronal cells expressing all three neuronal markers MAP2, TUJ1 and PSA-NCAM. Our data are also consistent with Bexell *et al.* indicating that PSA-NCAM expressing neuroblasts sparsely infiltrate into the tumor and are DCX positive (Bexell *et al.*, 2007). DCX positive and PSA-NCAM positive cells are present at the highest density in proximity to the SVZ and in the area between the SVZ and the tumor. In contrast, lower numbers of DCX and PSA-NCAM synthesizing cells with migratory morphology appear in the corpus callosum and on the lateral side of the tumor (Bexell *et al.*, 2007). To investigate DCX expression in glioma, we analyzed DCX expression in human primary glioma cells from different patients and from different grades, and in implanted DsRed-2 labeled U87 glioma tumor in nude rat. Our data demonstrate that glioma cells are DCX deficient. These DCX positive cells in glioma are either infiltrated neuroblasts or pre-existing neuronal cells. The migrating neuroblasts constitute the source for neuronal replacement in the striatum following tumor induced neuronal cell death (Bexell *et al.*, 2007). Thus, glioma cell invasion does not depend on DCX. In contrast, we demonstrated that DCX suppressed glioma cell invasion. Actin depolymerization appears to mediate DCX inhibition of glioma cell invasion. Cell migration depends on the actin dynamics, in which the rate of actin polymerization and depolymerization are important (Reviewed in ref. Ridley *et al.*, 2003). Actin polymerization influences cell migration and MMP expression. In contrast, actin depolymerization inhibits cell migration (Ridley *et al.*, 2003; Chintala *et al.*, 1999; 1997). Actin polymerization is regulated by phosphatase activity (Gu *et al.*, 2003; Oliver *et al.*, 2002). Our data demonstrated that DCX interacts with PP1, competes with actin polymerization reactions, suppresses specifically expression and activities of MMP2 and MMP9 and reduces glioma cell migration in vitro. However, MMP14 and CD44 that are known to be involved in glioma invasion (Bellail *et al.*, 2004, Shalinsky *et al.*, 1999) remained unaffected by DCX. DCX transfection induces migration for 3h in U87 cells, as previously reported (Santra *et al.*, 2006b). This apparent discrepancy in data can be resolved by analysis of the experimental conditions of both sets of experiments. When the scrape migration assay as in the present study, was performed for a longer period of time (6 and 12h) and a wider scrape of 1000 μl instead of 200 μl micro-pipette tip was employed, we found that DCX significantly inhibited U87 cell migration. DCX inhibits

phosphatase activity of PP1. DCX mediated depolymerization of actin inhibits glioma U87 cell invasion and reduces MMP2 and MMP9 expression. As neurabin II siRNA, MMP2siRNA and MMP9siRNA treatment does not completely reverse the DCX mediated suppression of glioma cell invasion, these data indicate that another mechanism, possibly induction of E-cadherin, a negative marker of tumor invasion (Xu and Yu 2003) by DCX transfection in U87 cells (Santra *et al.*, 2006b), may also be involved.

In conclusion, DCX reduces glioma cell invasion. A novel mechanism is also linked to DCX mediated glioma tumor suppression and inhibition of glioma cell invasion via PP1 pathway. DCX is phosphorylated by JNK in DCX synthesizing glioma U87 tumor cells (Santra *et al.*, 2006a). Phosphorylated DCX interacts with neurabin II and PP1 in the cytosol. Localization of DCX-Neurabin II-PP1 complex in the cytosol causes inhibition of phosphatase activities of PP1 that are involved in two mechanistic links of reduction of glioma tumor-associated progressions- 1) catastrophe in mitotic spindle checkpoint that leads to growth arrest in G2-M phase in cell cycle progression and 2) depolymerization of actin that leads to inhibition of glioma cell invasion.

## Acknowledgments

We thank Dr. Thomas Mikkelsen, Henry Ford Hospital, Detroit, MI for providing us human glioma cells and paraffin slides, Dr. Anthony N. van den Pol, Department of Neurosurgery, Yale University School of Medicine, New Haven, Connecticut for providing us primary human glioma cells, and Dr. Roger Davis, Biochemistry and Molecular Pharmacology, University of Massachussets Medical School, Worcester, Massachusetts for providing us expression vectors containing dominant negative acting mutants of JNK1 for providing us constitutively active expression vector of JNK 1 fused with MKK7.

## References

Alphey L, Parker L, Hawcroft G, Guo Y, Kaiser K, Morgan G. KLP38B: a mitotic kinesin-related protein that binds PP1. J Cell Biol 1997;138:395–409. [PubMed: 9230081]

Ahn MY, Zhang ZG, Tsang W, Chopp M. Endogenous plasminogen activator expression after embolic focal cerebral ischemia in mice. Brain Res 1999;837:169–176. [PubMed: 10433999]

Bellail AC, Hunter SB, Brat DJ, Tan C, Van Meir EG. Microregional extracellular matrix heterogeneity in brain modulates glioma cell invasion. Int J Biochem Cell Biol 2004;36:1046–1069. [PubMed: 15094120]

Bexell D, Gunnarsson S, Nordquist J, Bengzon J. Characterization of the subventricular zone neurogenic response to rat malignant brain tumors. Neuroscience 2007;147:824–832. [PubMed: 17583435]

Bielas SL, Serneo FF, Chechlacz M, Deerinck TJ, Perkins GA, Allen PB, Ellisman MH, Gleeson JG. Spinophilin facilitates dephosphorylation of doublecortin by PP1 to mediate microtubule bundling at the axonal wrist. Cell 2007;129:579–591. [PubMed: 17482550]

Blázquez C, Salazar M, Carracedo A, Lorente M, Egia A, González-Feria L, Haro A, Velasco G, Guzmán M. Cannabinoids inhibit glioma cell invasion by down-regulating matrix metalloproteinase-2 expression. Cancer Res 2008;68:1945–1952. [PubMed: 18339876]

Bowerman, Bruce. Cell division: timing the machine. Nature 2004;430:840–842. [PubMed: 15318203]

Castedo M, Perfettini JL, Roumier T, Kroemer G. Cyclin-dependent kinase-1: linking apoptosis to cell cycle and mitotic catastrophe. Cell Death Differ 2002;9:1287–1293. [PubMed: 12478465]

Chintala SK, Kyritsis AP, Mohan PM, Mohanam S, Sawaya R, Gokslan Z, Yung WK, Steck P, Uhm JH, Aggarwal BB, Rao JS. Altered actin cytoskeleton and inhibition of matrix metalloproteinase expression by vanadate and phenylarsine oxide, inhibitors of phosphotyrosine phosphatases: modulation of migration and invasion of human malignant glioma cells. Mol Carcinog 1999;26:274–285. [PubMed: 10569804]

Chintala SK, Mohanam S, Go Y, Venkaiah B, Sawaya R, Gokaslan ZL, Rao JS. Altered in vitro spreading and cytoskeletal organization in human glioma cells by downregulation of urokinase receptor. Mol Carcinog 1997;20:355–365. [PubMed: 9433480]

Corbo JC, Deuel TA, Long JM, LaPorte P, Tsai E, Wynshaw-Boris A, Walsh CA. Doublecortin is required in mice for lamination of the hippocampus but not the neocortex. J Neurosci 2002;22:7548–7557. [PubMed: 12196578]

Daou MC, Smith TW, Litofsky NS, Hsieh CC, Ross AH. Doublecortin is preferentially expressed in invasive human brain tumors. Acta Neuropathol 2005;110:472–80. [PubMed: 16195916]

Demuth T, Berens ME. Molecular mechanisms of glioma cell migration and invasion. J Neurooncol 2004;70:217–228. [PubMed: 15674479]

Eriksson D, Löfroth PO, Johansson L, Riklund KA, Stigbrand T. Cell cycle disturbances and mitotic catastrophes in HeLa Hep2 cells following 2.5 to 10 Gy of ionizing radiation. Clin Cancer Res 2007;13:5501s–5508s. [PubMed: 17875782]

Francis F, Koulakoff A, Boucher D, Chafey P, Schaar B, Vinet MC, Friocourt G, McDonnell N, Reiner O, Kahn A, McConnell SK, Berwald-Netter Y, Denoulet P, Chelly J. Doublecortin is a developmentally regulated microtubule-associated protein expressed in migrating and differentiating neurons. Neuron 1999;23:247–256. [PubMed: 10399932]

Gadde S, Heald R. Mechanisms and molecules of the mitotic spindle. Curr Biol 2004;14:R797–805. [PubMed: 15380094]

Garzon DJ, Fahnestock M. Oligomeric amyloid decreases basal levels of brain-derived neurotrophic factor (BDNF) mRNA via specific downregulation of BDNF transcripts IV and V in differentiated human neuroblastoma cells. J Neurosci 2007;27:2628–2635. [PubMed: 17344400]

Glass R, Synowitz M, Kronenberg G, Walzlein JH, Markovic DS, Wang LP, Gast D, Kiwit J, Kempermann G, Kettenmann H. Glioblastoma- induced attraction of endogenous neural precursor cells is associated with improved survival. J Neurosci 2005;25:2637–2646. [PubMed: 15758174]

Gu L, Zhang H, Chen Q, Chen J. Calyculin A-induced actin phosphorylation and depolymerization in renal epithelial cells. Cell Motil Cytoskeleton 2003;54:286–295. [PubMed: 12601691]

Hirose Y, Katayama M, Mirzoeva OK, Berger MS, Pieper RO. Akt activation suppresses Chk2-mediated, methylating agent-induced G2 arrest and protects from temozolomide-induced mitotic catastrophe and cellular senescence. Cancer Res 2005;65:4861–4869. [PubMed: 15930307]

Huang H, Fletcher L, Beeharry N, Daniel R, Kao G, Yen TJ, Muschel RJ. Abnormal cytokinesis after X-irradiation in tumor cells that override the G2 DNA damage checkpoint. Cancer Res 2008;68:3724–3732. [PubMed: 18483255]

Ianzini F, Domann FE, Kosmacek EA, Phillips SL, Mackey MA. Human glioblastoma U87MG cells transduced with a dominant negative p53 (TP53) adenovirus construct undergo radiation-induced mitotic catastrophe. Radiat Res 2007;168:183–92. [PubMed: 17638400]

Jackson JR, Patrick DR, Dar MM, Huang PS. Targeted anti-mitotic therapies: can we improve on tubulin agents? Nat Rev Cancer 2007;7:107–117. [PubMed: 17251917]

Jiang F, Chopp M, Katakowski M, Cho KK, Yang X, Hochbaum N, Tong L, Mikkelsen T. Photodynamic therapy with photofrin reduces invasiveness of malignant human glioma cells. Lasers Med Sci 2002;17:280–288. [PubMed: 12417983]

Livak KJ, Schmittgen TD. Analysis of relative gene expression data using real-time quantitative PCR and the 2(-Delta Delta C(T)) Method. Methods 2001;25:402–408. [PubMed: 11846609]

Liu G, Yuan X, Zeng Z, Tunici P, Ng H, Abdulkadir IR, Lu L, Irvin D, Black KL, Yu JS. Analysis of gene expression and chemoresistance of CD133+ cancer stem cells in glioblastoma. Mol Cancer 2006;5:67–78. [PubMed: 17140455]

Masui K, Mawatari SY, Suzuki SO, Iwaki T. Evaluation of sensitivity and specificity of doublecortin immunostatining for the detection of infiltrating glioma cells. Brain Tumor Pathol 2008;25:1–7. [PubMed: 18415660]

Monnet C, Correia K, Sarthou AS, Irlinger F. Quantitative detection of Corynebacterium casei in cheese by real-time PCR. Appl Environ Microbiol 2006;72:6972–6979. [PubMed: 16950905]

Moores CA, Perderiset M, Kappeler C, Kain S, Drummond D, Perkins SJ, Chelly J, Cross R, Houdusse A, Francis F. Distinct roles of doublecortin modulating the microtubule cytoskeleton. EMBO J 2006a; 25:4448–57. [PubMed: 16957770]

Moores CA, Milligan RA. Lucky 13-microtubule depolymerisation by kinesin-13 motors. J Cell Sci 2006b;119(Pt 19):3905–3913. [PubMed: 16988025]

Nomura M, Nomura N, Newcomb EW, Lukyanov Y, Tamasdan C, Zagzag D. Geldanamycin induces mitotic catastrophe and subsequent apoptosis in human glioma cells. J Cell Physiol 2004;201:374–384. [PubMed: 15389545]

Oliver CJ, Terry-Lorenzo RT, Elliott E, Bloomer WA, Li S, Brautigan DL, Colbran RJ, Shenolikar S. Targeting protein phosphatase 1 (PP1) to the actin cytoskeleton: the neurabin I/PP1 complex regulates cell morphology. Mol Cell Biol 2002;22:4690–4701. [PubMed: 12052877]

Ozduman K, Wollmann G, Piepmeier JM, van den Pol AN. Systemic vesicular stomatitis virus selectively destroys multifocal glioma and metastatic carcinoma in brain. J Neurosci 2008;28:1882–9183. [PubMed: 18287505]

Raingeaud J, Gupta S, Rogers JS, Dickens M, Han J, Ulevitch RJ, Davis RJ. Pro-inflammatory cytokines and environmental stress cause p38 mitogenactivated protein kinase activation by dual phosphorylation on tyrosine and threonine. J Biol Chem 1995;270:7420–7426. [PubMed: 7535770]

Ridley AJ, Schwartz MA, Burridge K, Firtel RA, Ginsberg MH, Borisy G, Parsons JT, Horwitz AR. Cell migration: integrating signals from front to back. Science 2003;302:1704–1709. [PubMed: 14657486]

Romanic AM, White RF, Arleth AJ, Ohlstein EH, Barone FC. Matrix metalloproteinase expression increases after cerebral focal ischemia in rats: inhibition of matrix metalloproteinase-9 reduces infarct size. Stroke 1998;29:1020–1030. [PubMed: 9596253]

Santra M, Santra S, Zhang J, Chopp M. Ectopic decorin expression up-regulates VEGF expression in mouse cerebral endothelial cells via activation of the transcription factors Sp1, HIF1alpha, and Stat3. J Neurochem 2008;105:324–337. [PubMed: 18021292]

Santra M, Zhang X, Santra S, Jiang F, Chopp M. Ectopic doublecortin gene expression suppresses the malignant phenotype in glioblastoma cells. Cancer Res 2006a;66:11726–11735. [PubMed: 17178868]

Santra M, Liu XS, Santra S, Zhang J, Zhang RL, Zhang ZG, Chopp M. Ectopic expression of doublecortin protects adult mouse progenitor cells and human glioma cells from severe oxygen and glucose deprivation. Neuroscience 2006b;142:739–752. [PubMed: 16962712]

Santra M, Katakowski M, Zhang RL, Zhang ZG, Meng H, Jiang F, Chopp M. Protection of adult mouse progenitor cells and human glioma cells by de novo decorin expression in an oxygen- and glucose-deprived cell culture model system. J Cereb Blood Flow Metab 2006c;26:1311–1322. [PubMed: 16467781]

Santra M, Skorski T, Calabretta B, Lattime EC, Iozzo RV. De novo decorin gene expression suppresses the malignant phenotype in human colon cancer cells. Proc Natl Acad Sci U S A 1995;92:7016–7020. [PubMed: 7624361]

Santra M, Mann DM, Mercer EW, Skorski T, Calabretta B, Iozzo RV. Ectopic expression of decorin protein core causes a generalized growth suppression in neoplastic cells of various histogenetic origin and requires endogenous p21, an inhibitor of cyclin-dependent kinases. J Clin Invest 1997;100:149–157. [PubMed: 9202067]

Santra M, Eichstetter I, Iozzo RV. An anti-oncogenic role for decorin. Down-regulation of ErbB2 leads to growth suppression and cytodifferentiation of mammary carcinoma cells. J Biol Chem 2000;275:35153–35161. [PubMed: 10942781]

Shalinsky DR, Brekken J, Zou H, McDermott CD, Forsyth P, Edwards D, Margosiak S, Bender S, Truitt G, Wood A, Varki NM, Appelt K. Broad antitumor and antiangiogenic activities of AG3340, a potent and selective MMP inhibitor undergoing advanced oncology clinical trials. Ann N Y Acad Sci 1999;878:236–270. [PubMed: 10415735]

Shmueli A, Gdalyahu A, Sapoznik S, Sapir T, Tsukada M, Reiner O. Site-specific dephosphorylation of doublecortin (DCX) by protein phosphatase 1 (PP1). Mol Cell Neurosci 2006;32:15–26. [PubMed: 16530423]

Soltani MH, Pichardo R, Song Z, Sangha N, Camacho F, Satyamoorthy K, Sangueza OP, Setaluri V. Microtubule-associated protein 2, a marker of neuronal differentiation, induces mitotic defects, inhibits growth of melanoma cells, and predicts metastatic potential of cutaneous melanoma. Am J Pathol 2005;166:1841–50. [PubMed: 15920168]

Taylor KR, Holzer AK, Bazan JF, Walsh CA, Gleeson JG. Patient mutations in doublecortin define a repeated tubulin-binding domain. J Biol Chem 2000;275:34442–34450. [PubMed: 10946000]

Tsukada M, Prokscha A, Eichele G. Distinct roles of PP1 and PP2A-like phosphatases in control of microtubule dynamics during mitosis. Biochem Biophys Res Commun 2006;343:839–847. [PubMed: 16564023]

Vile RG. Viral mediated cell fusion: viral fusion--the making, or breaking, of a tumour? Gene Ther 2006;13:1127–1130. [PubMed: 17243200]

Xu Y, Yu Q. E-cadherin negatively regulates CD44-hyaluronan interaction and CD44-mediated tumor invasion and branching morphogenesis. J Biol Chem 2003;10:8661–8668. [PubMed: 12511569]

Yamashita K, Yasuda H, Pines J, Yasumoto K, Nishitani H, Ohtsubo M, Hunter T, Sugimura T, Nishimoto T. Okadaic acid, a potent inhibitor of type 1 and type 2A protein phosphatases, activates cdc2/H1 kinase and transiently induces a premature mitosis-like state in BHK21 cells. EMBO J 1990;913:4331–4338. [PubMed: 2176149]

Zhang J, Li Y, Zheng X, Gao Q, Liu Z, Qu R, Borneman J, Elias SB, Chopp M. Bone marrow stromal cells protect oligodendrocytes from oxygen-glucose deprivation injury. J Neurosci Res 2008;86:1501–1510. [PubMed: 18214988]

Zhang X, Jiang F, Kalkanis SN, Yang H, Zhang Z, Katakowski M, Hong X, Zheng X, Chopp M. Combination of surgical resection and photodynamic therapy of 9L gliosarcoma in the nude rat. Photochem Photobiol 2006;82:1704–1711. [PubMed: 17007560]

Zhang Z, Jiang Q, Jiang F, Ding G, Zhang R, Wang L, Zhang L, Robin AM, Katakowski M, Chopp M. In vivo magnetic resonance imaging tracks adult neural progenitor cell targeting of brain tumor. Neuroimage 2004;23:281–287. [PubMed: 15325375]

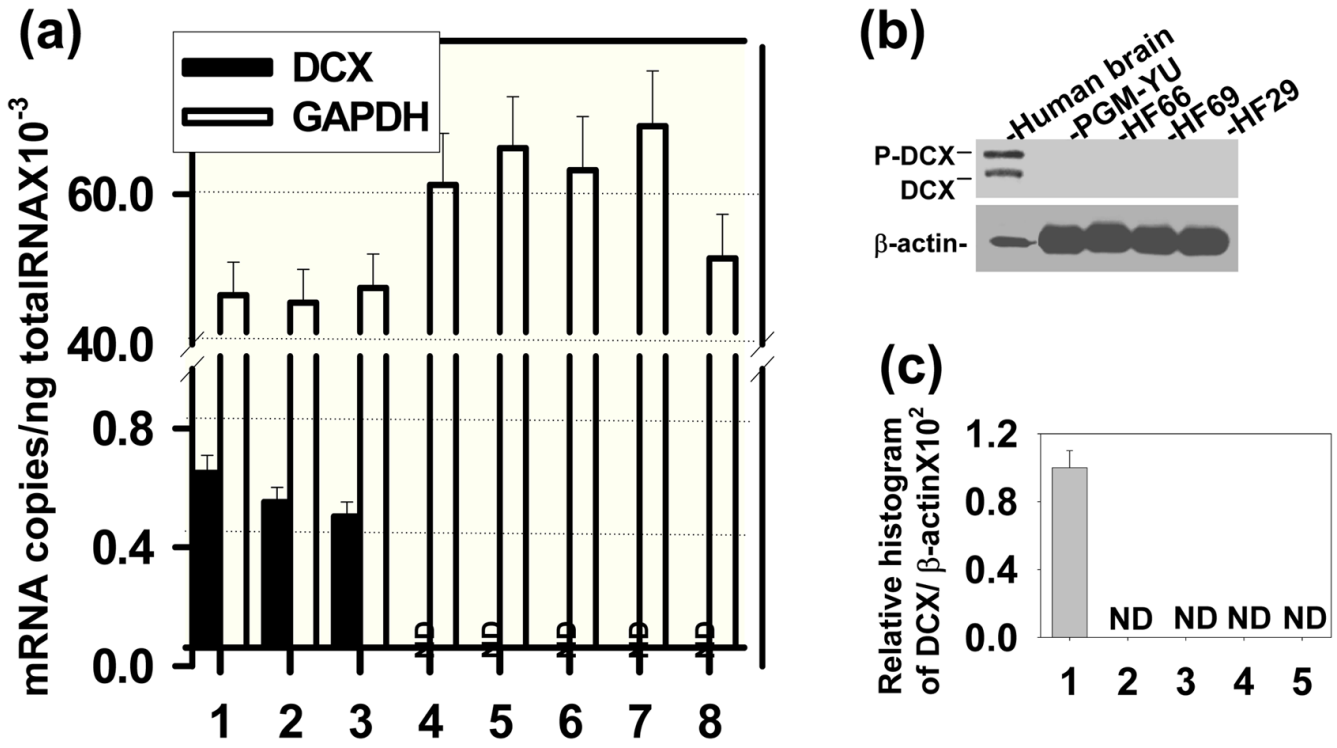


**Fig. 1.**

DCX expression is absent in glioma cells. (a) Absolute quantitative real time PCR was performed for DCX and GAPDH expression in total RNA extracted from 20, 30 and 50 years old normal human brains (1–3) and from human primary brain tumor cells such as primary glioblastoma multiforme, Yale University (PGM-YU) (4), primary glioblastoma multiforme (HF66) (5), anaplastic astrocytoma (HF69) (6), low grade astrocytoma (HF29) (7) and HEK 293T cells (8) cells. ND indicates not detectable. (b) Western blot was analyzed for DCX expression in normal human brain protein lysates (20μg) as positive control and 200μg protein lysates each from primary glioblastoma PGM-YU, HF66, HF69 and HF29 cells. Protein lysates were immunoblotted with DCX antibodies. DCX protein bands were detected by enhanced chemiluminescent (ECL) coupled to autoradiography. The loading of samples was normalized with β-actin. Migrations of DCX (DCX), phosphorylated DCX (P-DCX) and β-actin protein bands are marked in left. (c) DCX protein bands in three independent Western blots were quantified. ND indicates not detectable.

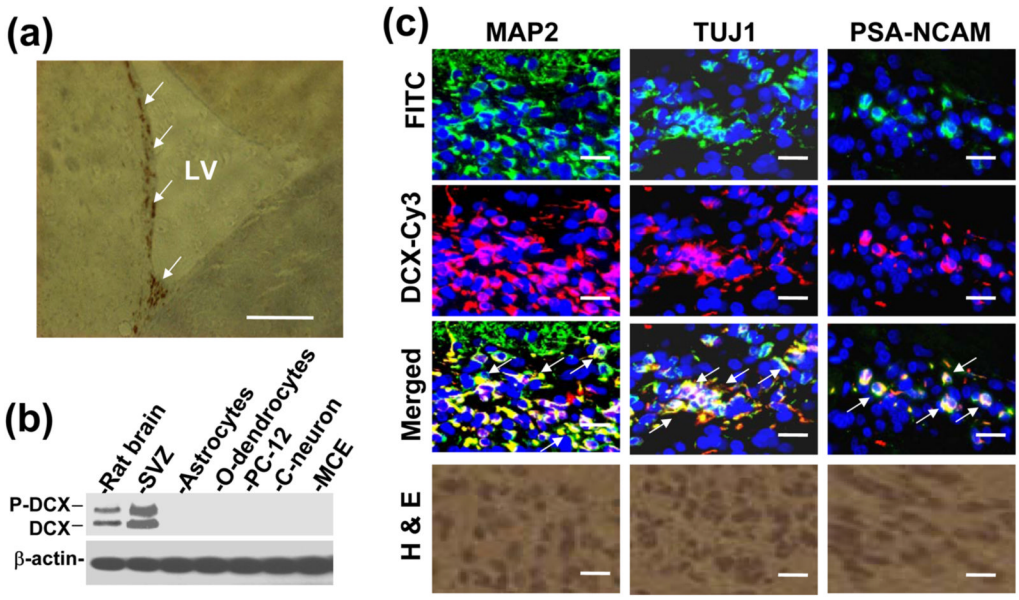


**Fig. 2.**

DCX expression in rat brain. (a) Paraffin sections of nude rat were immunostained with DCX antibody labeled with DAB. The arrows indicate DCX expression in the sub-ventricular zone lining the lateral ventricle (LV) wall. Scale bar of image = 250μm. (b) DCX expression in rat brain extracts, SVZ cells, rat astrocytes, mouse oligodendrocytes (o-dendrocyte), PC-12, mouse Cath.a neurons (C-neuron) and mouse cerebral endothelial (MCE) cells was analyzed by Western blot. (c) Paraffin sections of LV wall region of nude rat brain were double immunostained with FITC labeled neuronal markers such as MAP2, TUJ1 and PSA-NCAM, and Cy3 labeled DCX (DCX-Cy3) and counterstained with DAPI. Images are merged (Merged). Arrows indicate merged DCX and neuronal markers (MAP2, TUJ1 and PSA-NCAM) into yellow fluorescence. Alternate H&E staining of the corresponding images were shown at the bottom. Scale bar of images = 25μm.

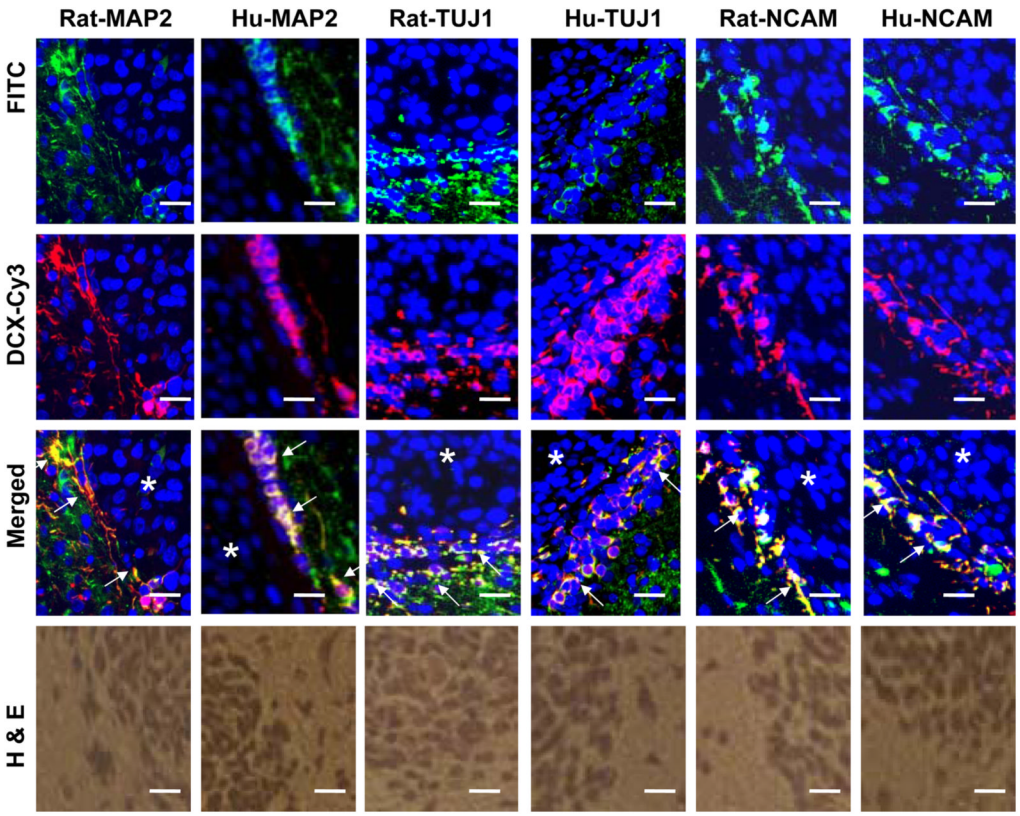


**Fig. 3.**

DCX positive neuroblasts are present in human and rat peritumor region of glioma. Paraffin sections of rat and human glioma tissues were double immunostained with FITC labeled neuron specific markers such as MAP2, TUJ1 and PSA-NCAM, and Cy3 labeled DCX and counterstained with DAPI. Images are merged. Asterisks indicate tumor (dense counterstained nuclei with DAPI). Arrows indicate the merged images of MAP2, TUJ1 and PSA-NCAM with DCX at the boundary of tumors. Alternate H&E staining of the corresponding images were shown at the bottom. Scale bar of images = 25μm.

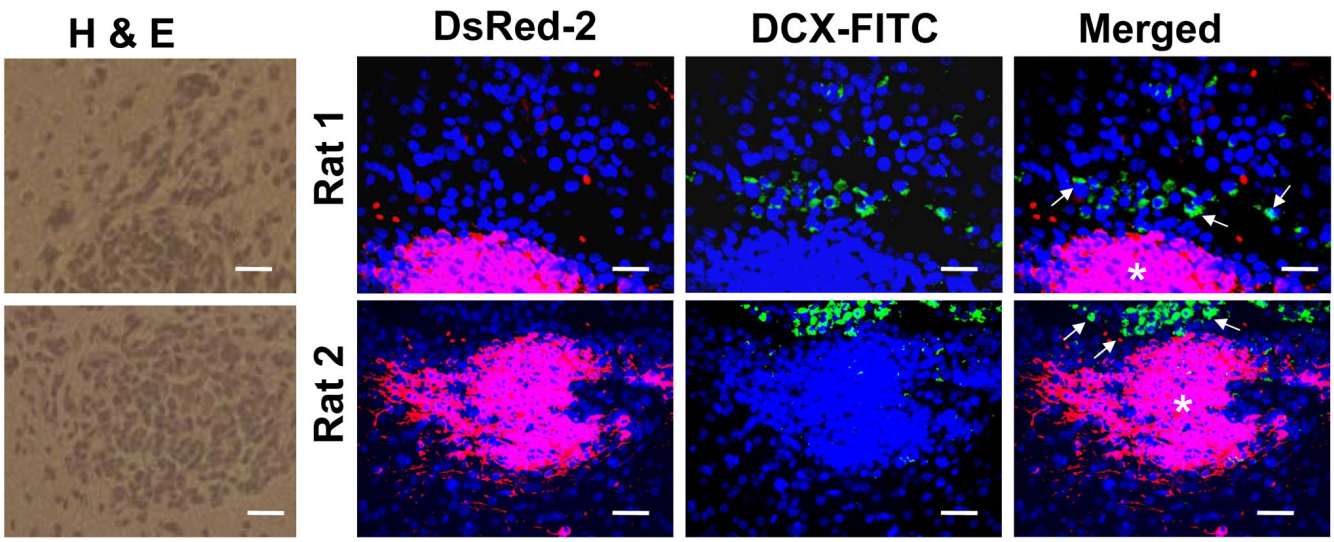


**Fig. 4.**

DCX positive cells are present in peritumor region of DsRed-2 labeled U87 glioma implanted in nude rat. The frozen brain sections (8 μm) were immunostained with FITC labeled DCX and counterstained with DAPI. Arrows indicate DCX expressing cells present in peritumor region of DsRed-2 labeled U87 glioma implanted in both nude rats. Alternate H&E staining of the corresponding images were shown at the left. Scale bar of images = 100μm.

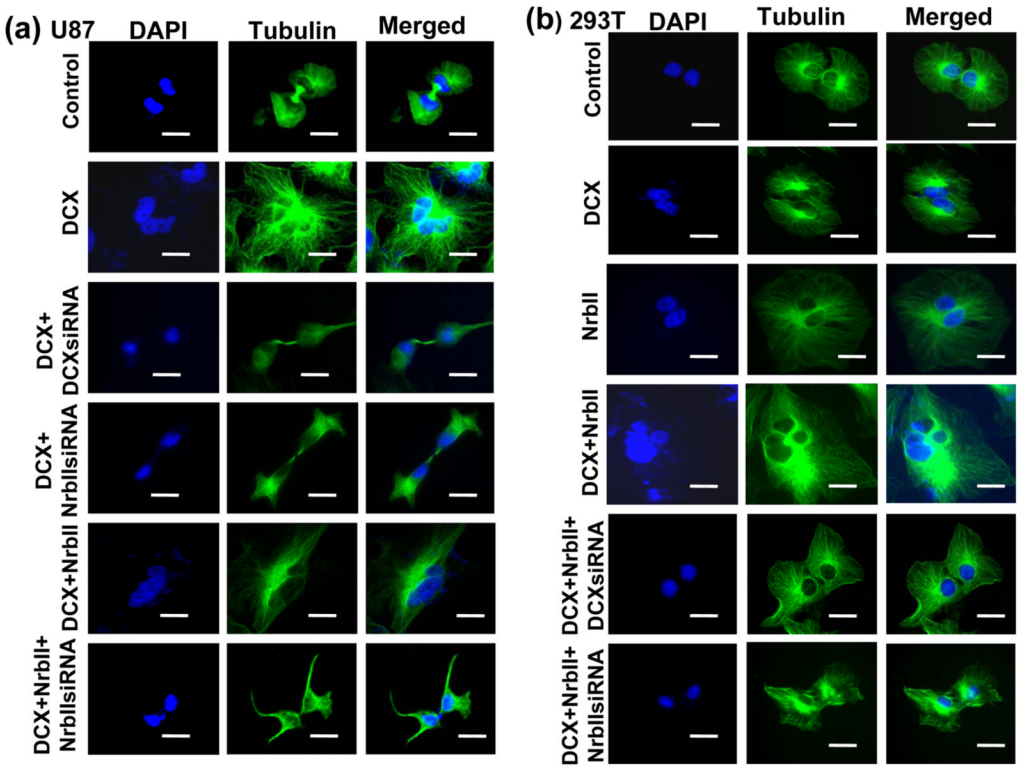


**Fig. 5.**

DCX induces mitotic spindle catastrophe. Mitotic tubulins were immunostained with monoclonal α-tubulin antibodies followed by antimouse IgG–FITC and counterstained with DAPI in mock (Control), DCX (DCX) transfected, DCXsiRNA lentivirus infected DCX synthesizing (DCX+DCXsiRNA), transiently neurabin II siRNA transfected DCX positive (DCX+ NrbIIsiRNA), NrbII transiently transfected DCX synthesizing, neurabin II siRNA treated DCX+Nrb II transfected (DCX+Nrb II+NrbIIsiRNA) U87 cells (a), and mock (Control), DCX (DCX), NrbII (NrbII) transfected, NrbII transiently transfected DCX synthesizing (DCX+NrbII), DCXsiRNA treated DCX+NrbII synthesizing (DCX+NrbII +DCXsiRNA) and NrbIIsiRNA treated DCX+NrbII synthesizing (DCX+NrbII+NrbIIsiRNA) HEK 293T cells (b). Scale bar of images = 5μm.

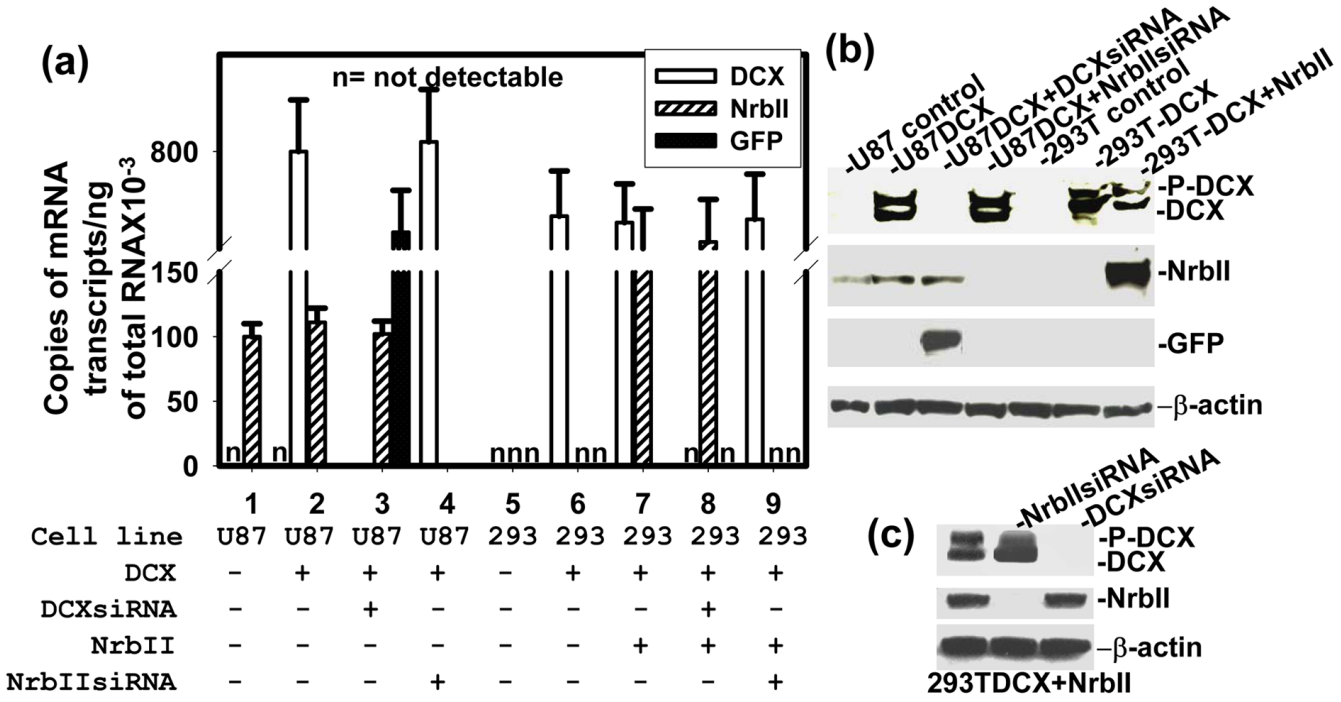


**Fig. 6.**

Analysis mRNA and proteins in transfected cells. Expression and knockdown of DCX, NrbII and GFP are analyzed by absolute qrtPCR in the transfected cells (shown at the bottom) (a). 'n' indicates that copies of mRNA are not detected. In Western blot, the transfected cells are shown at top (b), top and bottom (c) of the gel. Migration of protein bands are marked in right. The loading of samples was normalized with β-actin.

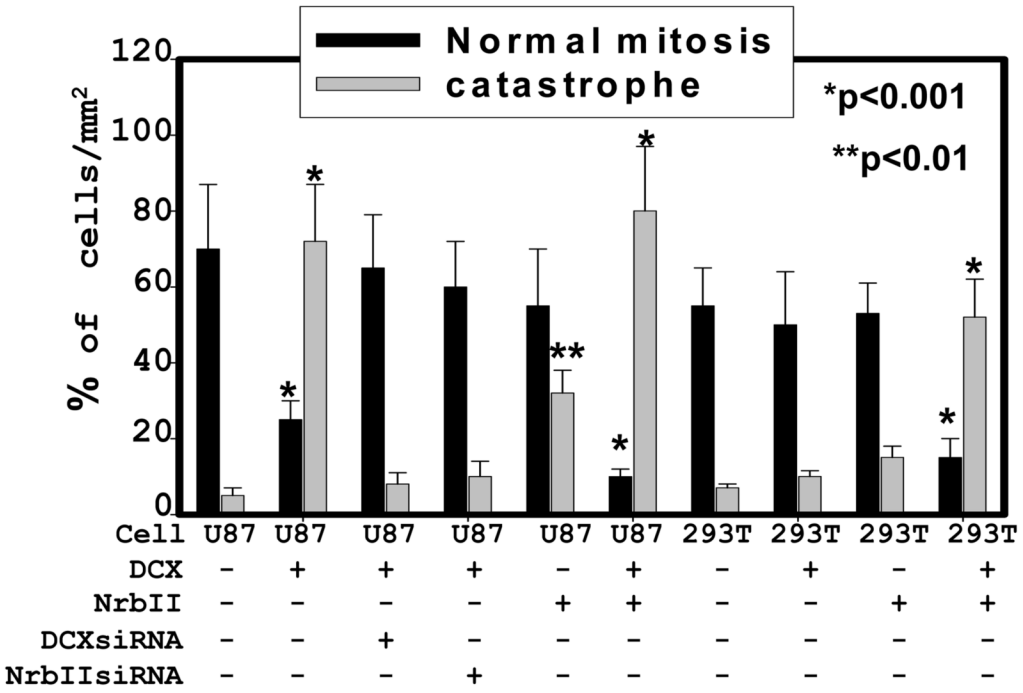


**Fig. 7.**

DCX transfection inhibits mitosis in U87 cells. Mitotic and catastrophic cells were quantified by counting the dividing cells with classic bipolar spindle poles/mm$^2$ area and multinucleated non-dividing cells/mm$^2$ area respectively. The percentages of normal mitotic and catastrophic cells were analyzed in U87 and HEK 293T cells transfected with plasmids conataining no insert (−), DCX insert (DCX), NrbII insert (NrbII), DCXsiRNA cassette (DCXsiRNA) and neurabin II siRNA cassette (NrbIIsiRNA) shown at the bottom. Asterisk indicates significance values. $P < 0.05$ was considered as significant.

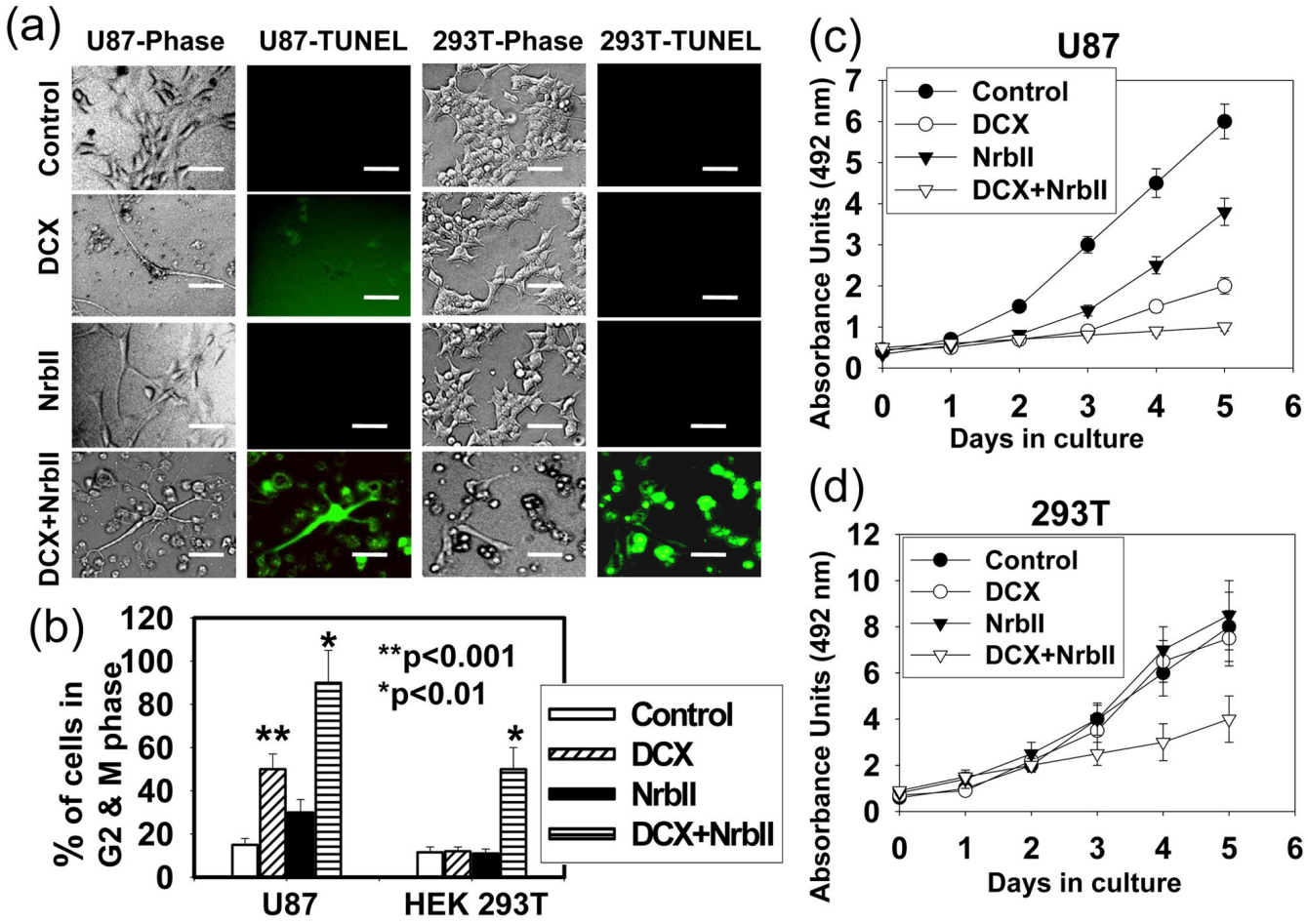


**Fig. 8.**

DCX synthesis and NrbII induces apoptosis. (a) TUNEL assay was performed in control, DCX (DCX), NrbII (NrbII), transiently (DCX+NrbII) transfected U87 and HEK 293T cells and examined under phase contrast (Phase) and fluorescence microscope for TUNEL staining (TUNEL). Scale bar of images = 20μm. (b) Bar graph represents the cells in G2-M phase of cell cycle quantified by FACS analysis. The proliferation assays were performed in control, DCX (DCX), NrbII (NrbII), transiently (DCX+NrbII) transfected U87 (c) and HEK 293T (d) cells.

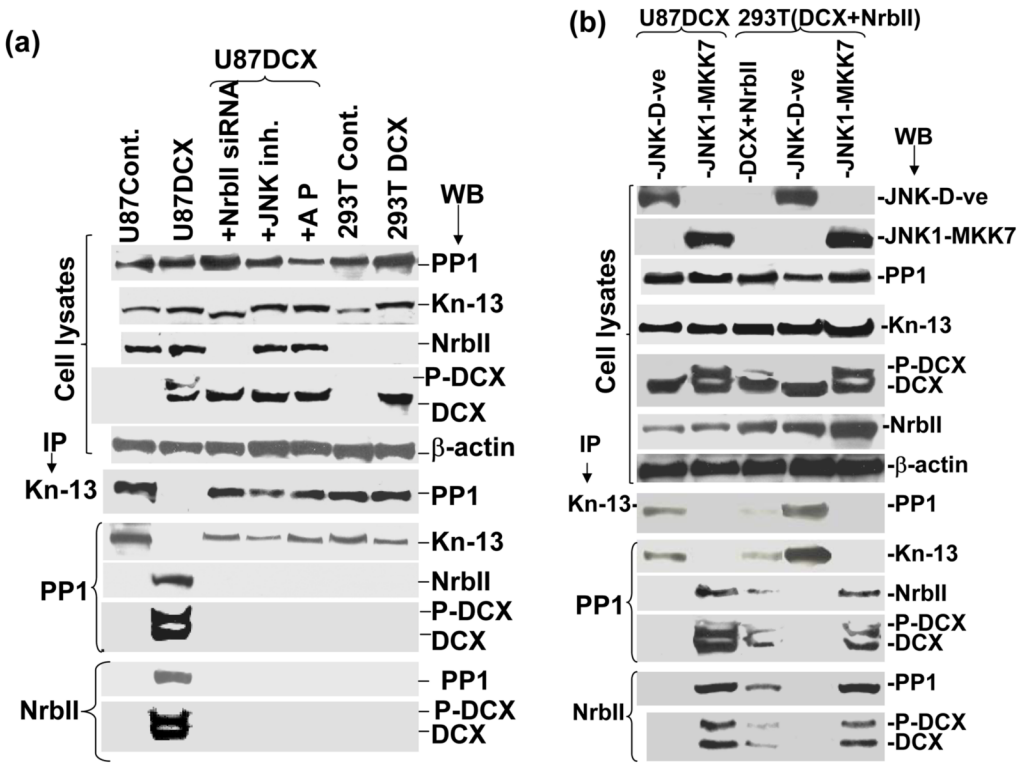


**Fig. 9.**

DCX interacts with PP1 in the cytosol. (a) Protein lysates extracted from mock transfected U87 cells (U87Cont.), DCX transfected U87 cells (U87DCX), DCX synthesizing U87 (U87DCX) cells either transiently transfected with plasmid containing neurabin II siRNA cassette (+NrbII siRNA) or treated with JNK specific inhibitor (+JNK inh.) or treated with alkaline phosphatase (+AP), mock transfected HEK293T cells (293T Cont.) and DCX transfected HEK293T (293T DCX) cells were analyzed by Western blot of input control cell lysates and immunoprecipitated (IP) with antibodies (indicated by arrow) against either kinesin-13 or PP1 or neurabin II (NrbII). (b) Western blot was analyzed in protein lysates extracted from JNK1 dominant negative expression vector transfected (JNK-D-ve) and JNK1-MKK7 expression vector transfected U87 and HEK 293T cells and transiently NrbII transfected DCX synthesizing HEK 293T cells. Equal amount (2.5 mg) of protein lysates were IP with antibodies (indicated by arrow) against either kinesin-13 or PP1 or neurabin II (NrbII). Amount of immunoprecipitation and protein-protein interaction were evaluated by sequential western blotting (WB) with antibodies (indicated by arrow) against PP1, kinesin-13, NrbII and DCX. Enhanced chemiluminescence (ECL) coupled to autoradiography detected protein bands. Note that there are no protein bands in both DCX and NrbII expressing U87 and HEK 293T cells for blotting with PP1 in IP with kinesin-13 and blotting with kinesin-13 in IP with PP1 indicating that PP1 does not interact with kinesin-13.

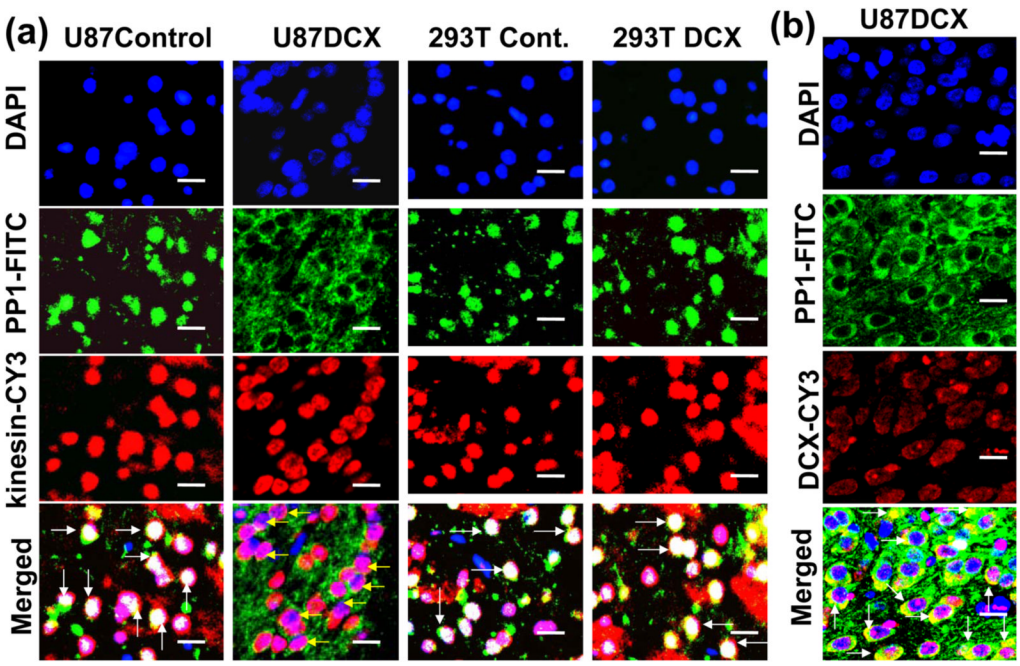


**Fig. 10.**

DCX induces localization of PP1 in the cytosol. (a) Nuclear staining with DAPI (DAPI), immunofluorescence staining of PP1 labeled with FITC (PP1-FITC), kinesin-13 labeled with CY3 (kinesin-CY3), and merged images (Merged) of the nuclear staining, PP1 and Kinesin-13 are indicated in mock (U87Control), DCX transfected U87 (U87DCX), mock (293T Cont.) and DCX transfected HEK 293T (293T DCX) cells. The white arrows indicate the merged images of nuclei, PP1 and Kinesin-13 (the mixture of blue, green and red fluorescence) as nuclear localization of PP1 and kinesin-13 in control U87, 293T and DCX transfected 293T cells. The yellow arrows indicate the merged images of nuclei and kinesin-13 (the mixture of blue and red fluorescence) as nuclear localization of kinesin-13 only in DCX transfected U87 cells. (b) In DCX transfected U87 (U87DCX) cells, nuclear staining with DAPI (DAPI), double immunofluorescence of PP1 labeled with FITC (PP1-FITC) and DCX labeled with CY3 (DCX-CY3), and merged images of PP1 and DCX, and counterstaining with DAPI are shown. The arrows indicate yellow fluorescence (the mixture of green and red) and merged images of PP1 and DCX as localization of DCX and PP1 in the cytosol of DCX transfected U87 cells. Scale bar of images = 20μm.

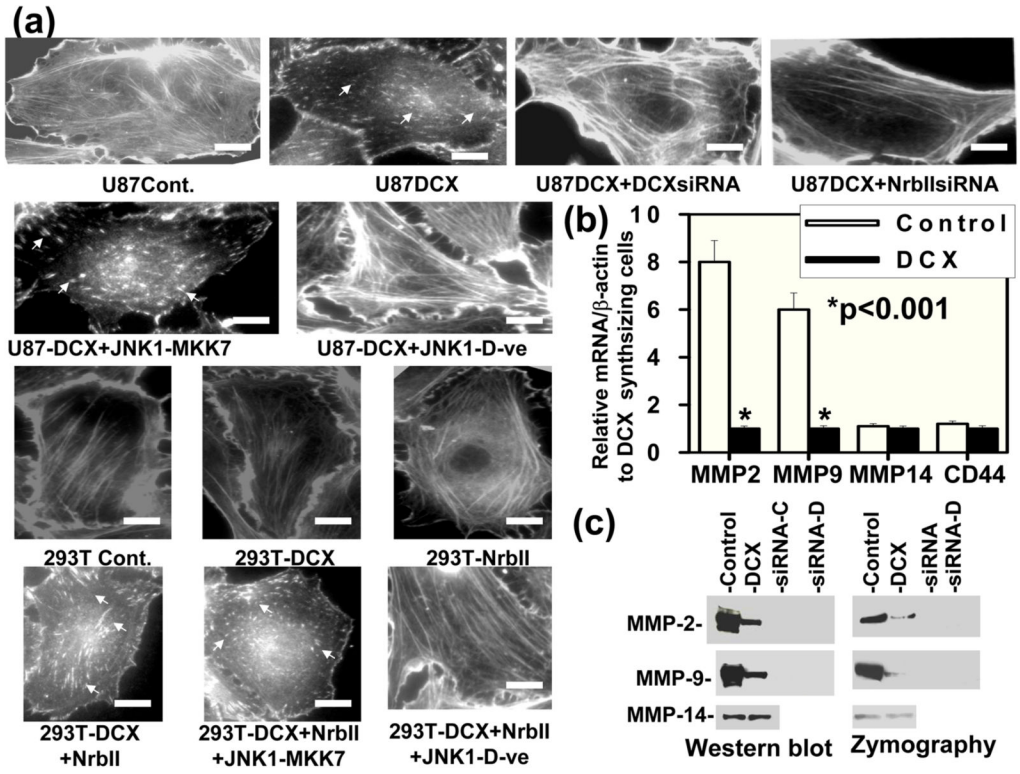


**Fig. 11.**

DCX synthesis induces actin depolymerization, suppresses the expression and activation of MMP2 and MMP9 in U87 cells and inhibits glioma cell invasion. (a) Actin filaments were stained with isothiocyanate-Phalloidin in control (U87-Cont.), DCX transfected (U87-DCX) cells, D CXsiRNA and NrbIIsiRNA transfected DCX synthesizing U87 cells (U87DCX +DCXsiRNA and U87DCX+NrbIIsiRNA) as well as control (293T-Cont.), DCX (293T-DCX), NrbII (293T-NrbII), DCX+NrbII (293T-DCX+NrbII) and NrbII+JNK1-MKK7 (293T-DCX+NrbII+JNK1-MKK7) transfected HEK 293T cells. Arrows indicate actin depolymerization both in DCX and NrbII synthesizing cells. Scale bar of images = 3μm. (b) Bar graph indicates relative qrtPCR analysis for mRNA expression of MMP2, MMP9, MPP14 and CD44 in mock transfected U87 cells (control) relative to their expression in DCX transfected U87 cells (DCX). Asterisk indicates significance values ($P < 0.001$). (c) Gels indicate the Western blot (Western blot) and zymography analysis (zymography) of MMP2, MMP9 and MMP14 in mock transfected (control), DCX transfected U87 (DCX), corresponding siRNA transfection in control (siRNA-C) and DCX synthesizing U87 (siRNA-D) cells. Equal amount of proteins (100 μg) was utilized for analysis. Notice that both expression and activation of MMP2 and MMP9 were significantly reduced in DCX transfected U87 cells in compared to control.

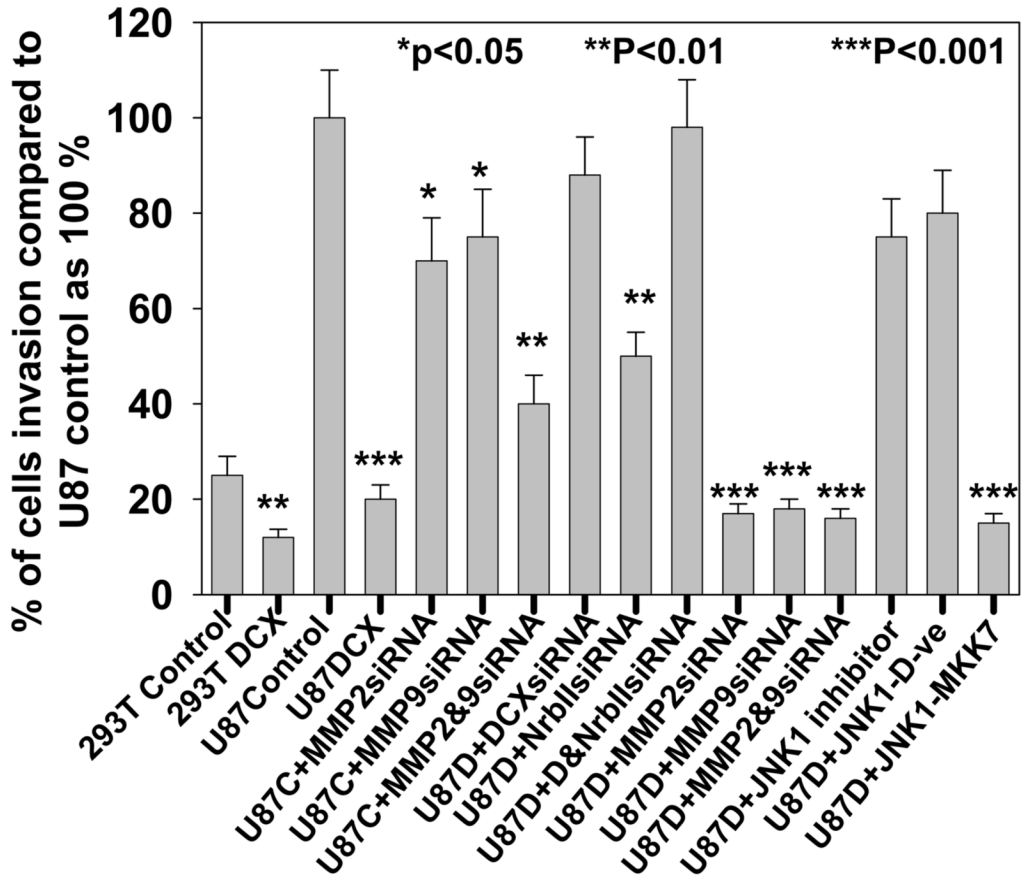


**Fig. 12.**

DCX inhibits glioma cell invasion in matrigel cell invasion analysis. In bar graph, matrigel cell invasion was analyzed in mock (293T control) and DCX transfected HEK293T (293T DCX) cells for 72h incubation, and in control (U87 control) and DCX transfected U87 (U87DCX) for 24h incubation. U87 cells transfected either with MMP2siRNA or MMP9siRNA (U87C +MMP2siRNA or U87C+MMP9siRNA), U87 cells transfected both with MMP2siRNA and MMP9siRNA (U87C+MMP2&9siRNA), DCX synthesizing U87 cells transfected either with MMP2siRNA or MMP9siRNA (U87D+MMP2siRNA or U87D+MMP9siRNA), DCX synthesizing U87 cells transfected both with MMP2siRNA and MMP9siRNA (U87D +MMP2&9siRNA) were examined for matrigel cell invasion assay for 24h incubation. In DCX synthesizing U87 cells, the effect of JNK1 inhibitor treatment (U87D+ JNK1 inhibitor), JNK1 dominant negative mutant transfection (U87D+ JNK1-D-ve) and constitutively active JNK1-MKK7 transfection were analyzed by matrigel cell invasion assay for 24h incubation. Asterisk indicates significance values. $P < 0.05$ was considered as significant.

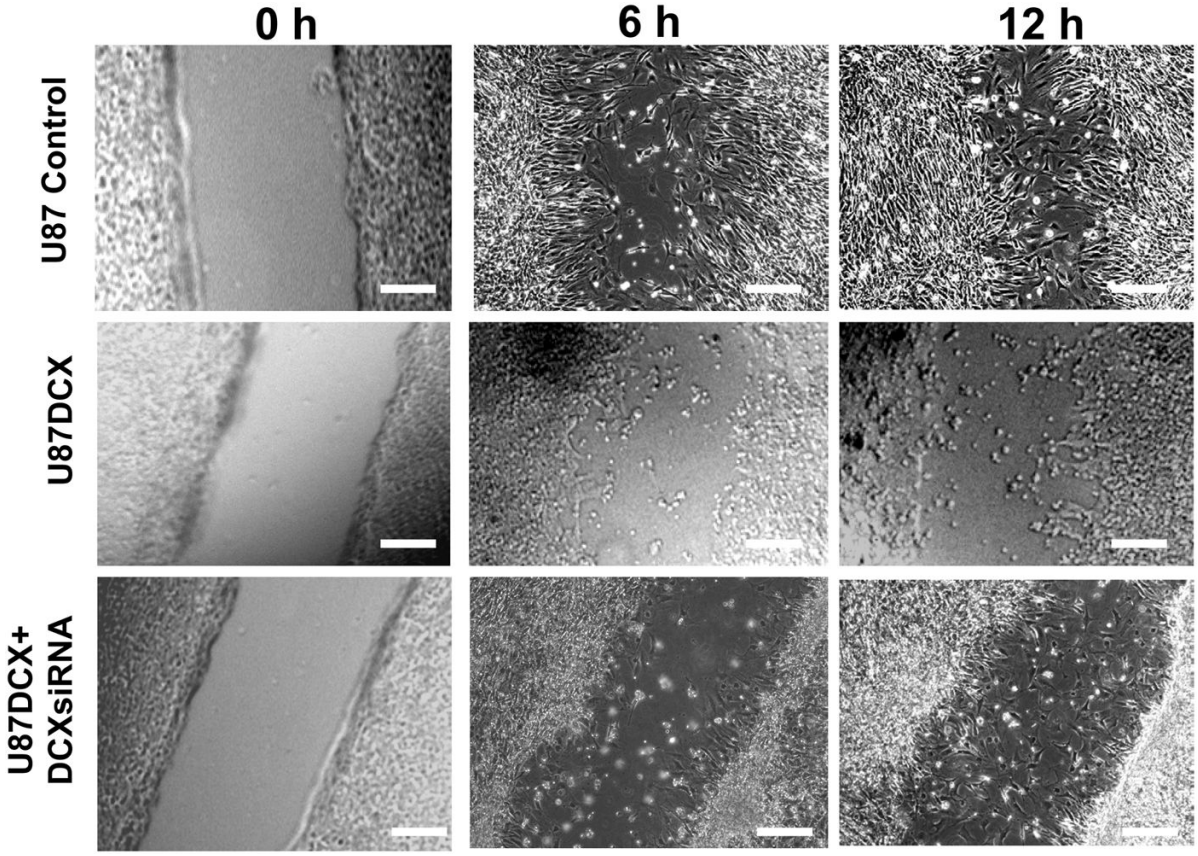


**Fig. 13.**

DCX synthesis reduces U87 cell migration in scrape migration assay. Scrape migration of control U87 (U87 control), DCX synthesizing U87 (U87DCX) and DCXsiRNA transfected DCX synthesizing U87 cells (U87DCX+DCXsiRNA) were analyzed at 0h, 6h and 12h incubations. Scale bar of images = 150μm.

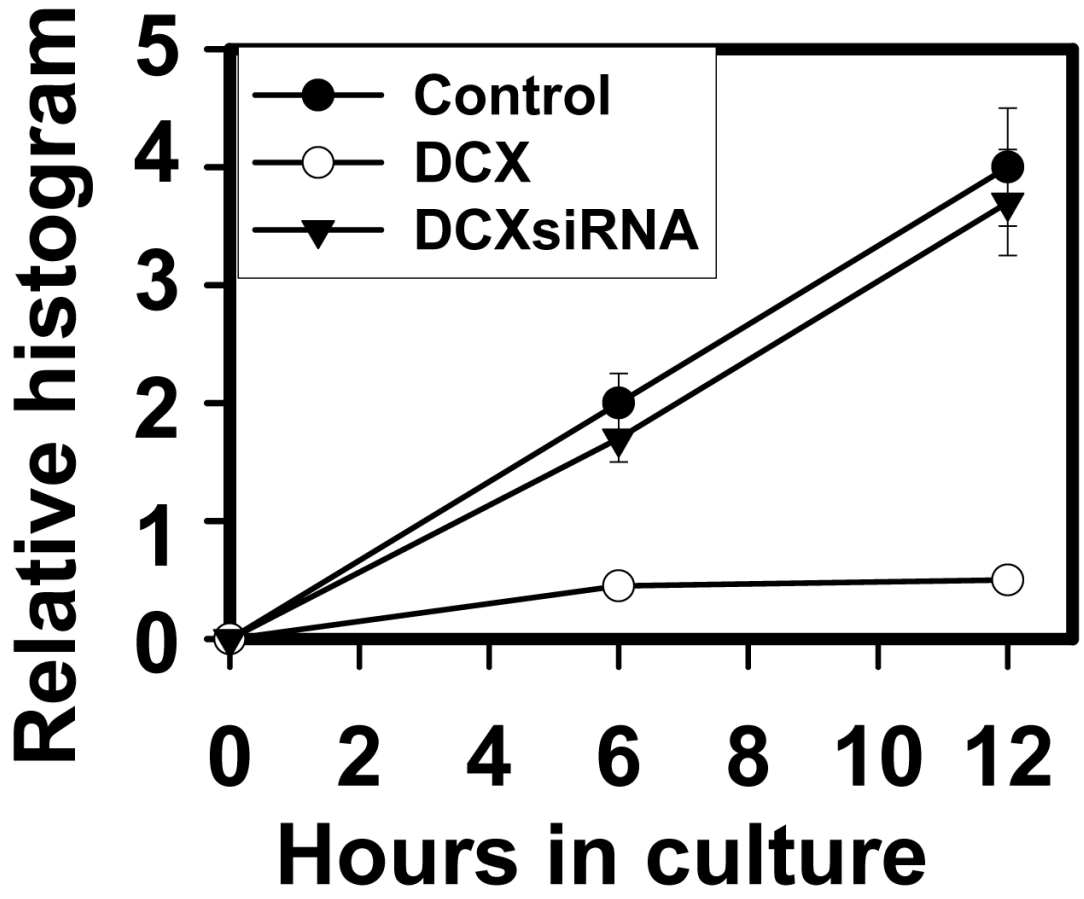


**Fig. 14.**

Quantitative analysis of scrape migration. Bar graph indicates quantitative analysis of scrape migration of control U87 (Control), DCX transfected U87 (DCX) and DCXsiRNA transfected DCX synthesizing U87 cells (DCXsiRNA) from 0h to 12h incubations.